3

Pattern Transfer with Additive Techniques

As an adolescent, I aspired to lasting fame, I craved factual certainty, and I thirsted for a meaningful vision of human life—so I became a scientist. This is like becoming an archbishop so you can meet girls.

Matt Cartmill

If any student comes to me and says he wants to be useful to mankind and go into research to alleviate human suffering, I advise him to go into charity instead. Research wants real egotists who seek their own pleasure and satisfaction, but find it in solving the puzzles of nature.

Albert Szent-Györgi

In science, the credit goes to the man who convinces the world, not to the man to whom the idea first occurs.

Francis Darwin

Introduction

Solids can be deposited onto a substrate from a liquid, a plasma, a gas, or a solid state. These additive techniques are often accompanied or followed by thermal processing to obtain desired materials properties and substrate adhesion. Although deposition methods, especially in the thin film arena, are generally the same as in integrated circuits (ICs), additive processes in miniaturization science span a much wider range from inorganic to organic materials. Besides the typical microelectronic elements (Si, Al, Au, Ti, W, Cu, Cr, O, N, and Ni-Fe alloys), miniaturization science involves deposition of several atypical elements such as Zr, Ta, Ir, C, Pt, Pd, Ag, Zn, and Nb (Inset 3.1). Moreover, a plethora of exotic compounds ranging from enzymes to shape memory alloys and from hydrogels to piezoelectrics are used. The number of materials and compounds involved in IC fabrication, in comparison, is very limited. In miniaturization science, particularly in chemical sensors and biomedical devices, modular, thick film technologies are more prevalent.

Before introducing additive processes such as CVD and PVD, we cover Si growth, doping, and oxidation. During the growth of a single Si crystal, no addition is involved; only a phase change takes place. An understanding of the physical nature of Si growth is important in understanding the dependence on crystallography of Si bulk micromachining as dealt with in Chapter 4. Doping of Si adds tiny amounts of special impurities to the crystal, dramatically altering its conductivity. Growth of a film, as in oxidation of Si in an oxygen atmosphere and nitridation of Si in ammonia, also differs from straight deposition due to the consumption of the substrate surface while forming the film. Silicon oxidation, like Si crystal growth, is a primary process. Understanding the Si/SiO_2 interface is essential for IC manufacture as well as for sensors such as ion-sensitive field effect transistors (ISFETs) and charge-coupled devices (CCDs).

Table 3.1 presents additive processes; Table 3.2 lists MEMS materials, typical deposition techniques, and an example application for the deposit. The references in Table 3.1 are meant as a basis for further study of additive processes.

In the deposition methods from the gas phase listed in Table 3.1, two major categories can be distinguished: direct line-of-sight impingement deposition techniques, called *physical vapor deposition* (PVD), and diffusive-convective mass transfer techniques, i.e., *chemical vapor deposition* (CVD). Evaporation, sputtering, molecular beam epitaxy (MBE), laser ablation deposition, ion plating, and cluster deposition represent the PVD techniques discussed. CVD techniques covered are plasma-enhanced (PECVD), atmospheric pressure (APCVD), low-pressure (LPCVD), very low pressure (VLPCVD), electron cyclotron resonance (ECRCVD), metallorganic (MOCVD), and spray

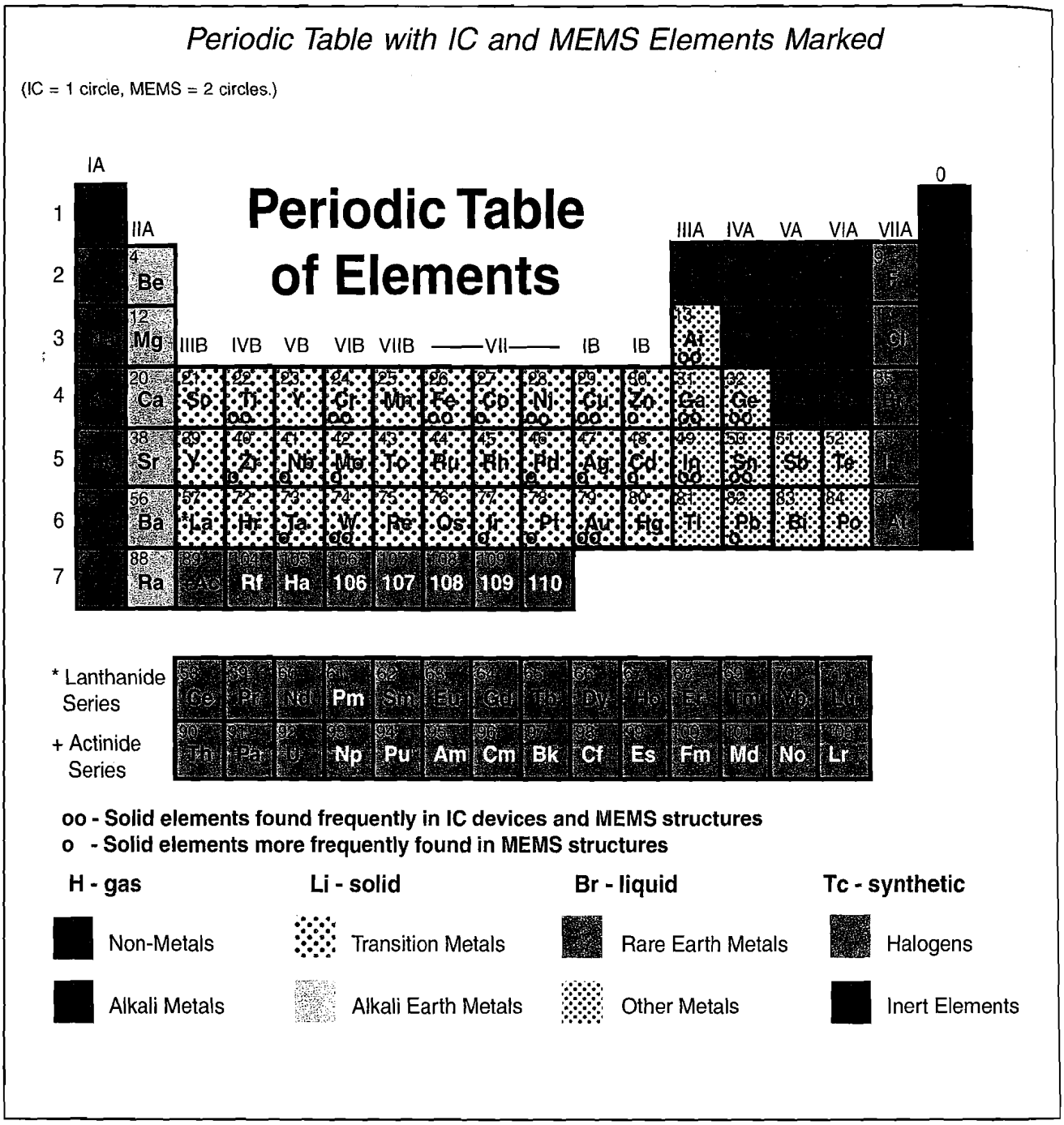

Inset 3.1 (This figure also appears as a color plate inside the front cover.)

pyrolysis. Epitaxial techniques have gained importance in ICs and mechanical sensor fabrication, and a separate section reviews progress in epitaxial methods. A particulate deposition technique, such as plasma spraying, is treated because of its potential chemical sensor applications. Like spray pyrolysis, plasma spraying does not have IC industry applications but might propel planar thick film chemical sensors into the realm of "batch" manufacturability.

With the growth of the BIOMEMS field, techniques for depositing organic materials for chemical and biological sensors, often arranged in some type of an array configuration, are gaining importance. In the last section of this chapter we review techniques with special merit for chemical and biological sensor manufacture. This includes spin coating, dip coating, plastic spraying, casting, Doctor's blade or tape casting, silk-screening, plasma polymerization, and Langmuir–Blodgett deposition. For sensor array manufacture, lithography, ink-jetting, mechanical microspotting, digital mirror deposition and electrochemical deposition of functional chemistries are highlighted.

As in the case of subtractive processes (Chapter 2), only the underlying physical and chemical principles of the various additive processes are explained. A limited number of examples of deposition processes in micromachining are given at the end of

TABLE 3.1 Additive Processes

Additive	Application	Reference
Bonding techniques	7740 glass to silicon	1
Casting	Thick resist (10–1000 μm)	
Chemical vapor deposition	Tungsten on metal	2
Dip coating	Wire-type ion selective electrodes	
Droplet delivery systems	Epoxy, chemical sensor membranes	
Electrochemical deposition	Copper on steel	3
Electroless deposition	Vias	4
Electrophoresis	Coating of insulation on heater wires	
Electrostatic toning	Xerography	
Ion cluster deposition		5
Ion implantation and diffusion of dopants	Boron into silicon	6
Ion plating	Metal on insulators	5
Laser deposition	Superconductor compounds	7
Liquid phase epitaxy (CVD)	GaAs	7
Material transformation (oxidation, nitridation, etc.)	Growth of SiO_2 on silicon	9
Molecular beam epitaxy (PVD)	GaAs	10
Plastic coatings	Electronics packages	11
Screen printing	Planar ion selective electrodes (ISEs)	12
Silicon crystal growth	Primary process	13
Spin-on	Thin resist (0.1–2 μm)	13
Spray pyrolysis (CVD)	CdS on metal	14
Sputter deposition (PVD)	Gold on silicon	15
Thermal evaporation (PVD)	Aluminum on glass	15
Thermal spray deposition from plasmas or flames	Coatings for aircraft engine parts and ZrO_2 sensors	16
Thermomigration	Aluminum contacts through silicon	17

the chapter; more examples and further discussion of properties of resulting films are dealt with in subsequent chapters.

Electrochemical and electroless metal deposition and micromolding are gaining renewed interest because of the emerging importance of replication methodologies. Those methods are dealt with separately in Chapter 6, on LIGA and other replication methods.

Silicon Growth

Silicon crystal growth constitutes the primary process toward the construction of most ICs and many micromachines. In the Czochralski crystal pulling method (Inset 3.2),[8] a silicon crystal seed is grown into a silicon single crystal by pulling it slowly upward, at about 2 to 5 cm/hr, from a molten and ultrapure silicon melt (Si melts at 1414°C). The molten silicon slowly rotates, nested in a silica crucible while pulling the growing crystal up. The melt must not be stirred; otherwise, oxygen is transported from the SiO_2-Si (crucible/liquid) interphase to the Si (liquid)-Si (solid) interphase. To avoid all contact with the crucible, eliminating, for example, most oxygen impurities, float-zone crystal growth (Inset 3.3)[18] is used instead. This

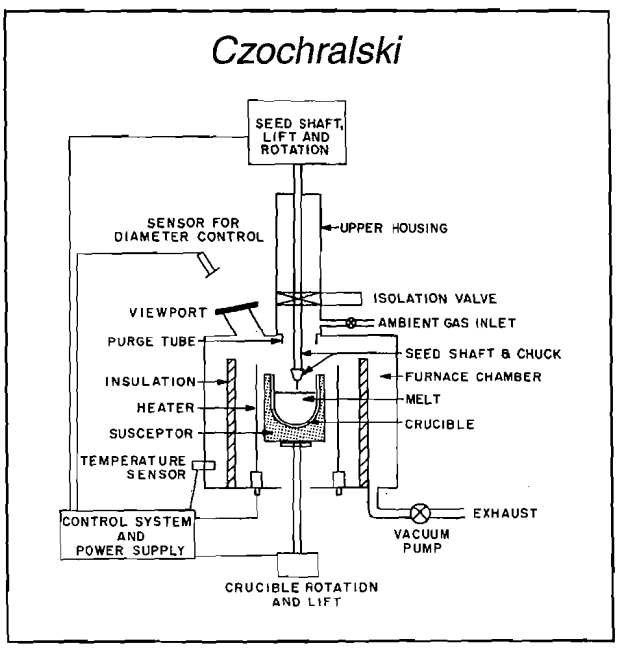

Inset 3.2

TABLE 3.2 IC and MEMS Materials, Deposition Method, and Typical Applications

Material	Deposition Technique	Function
Organic thin films		
Hydrogel	Silk-screening	Internal electrolyte in chem. sensors
Photoresist	Spin-on	Masking, planarization
Polyimide	Spin-on	Electrical isolation, planarization, microstructures
Metal oxides		
Aluminum oxide	CVD, sputtering, anodization	Electrical isolation
Indium oxide	Sputtering	Semiconductor
Tantalum oxide	CVD, sputtering, anodization	Electrical isolation
Tin oxide (SnO_2)	Sputtering	Semiconductor in gas sensors
Zinc oxide	Sputtering	Electrical isolation, piezoelectric
Noncrystalline silicon compounds		
α-Si-H	CVD, sputtering, plasma CVD	Semiconductors
Polysilicon	CVD, sputtering, plasma CVD	Conductor, microstructures
Silicides	CVD, sputtering, plasma CVD, alloying of metal and silicon	Conductors
Metals (thin films) with ρ in μΩ-cm in ( )		
Silver (Ag) (1.58)	Evaporation; sputtering	Electrochemistry electrode
Aluminum (Al) (2.7)	Evaporation, sputtering, plasma CVD	Electrical interconnects, limited to operations below 300°C
Chromium (Cr) (12.9)	Evaporation, sputtering, electroplating	Electrical conduction, adhesion layer (10–100nm)
Gold (Au) (2.4)	Evaporation, sputtering, electroplating	Electrical interconnects for higher temperatures than Al, optical reflection in the IR
Iridium (Ir) (5.1)	Sputtering	Electrochemistry electrode, biopotential measurements
Molybdenum	Sputtering	Electrical conduction
Platinum (Pt) (10.6)	Sputtering	Electrochemistry electrode, biopotential measurements
Palladium (Pd) (10.8)	Sputtering	Electrical conduction, adhesion layer, electrochemistry electrode, solder wetting layer
Tungsten (W) (5.5)	Sputtering	Electrical interconnects at higher temperatures
Titanium (Ti) (42)	Sputtering	Adhesion layer
Copper (Cu) (1.7)	Sputtering	Low resistivity interconnects
Alloys		
Al-Si-Cu	Evaporation, sputtering	Electrical conduction
Nichrome (NiCr) (200–500)	Evaporation, sputtering	Thin film laser-trimmed resistor
Permalloy™ (Ni_xFe_y)	Sputtering	Magnetoresistor, thermistor
TiNi (80)	Sputtering	Shape memory alloy
Chemically/physically modified silicon		
n/p type silicon	Implantation, diffusion, incorporation in the melt	Conduction modulation, etch stop
Porous silicon	Anodization	Electr. isolation, light-emitting structures, porous junctions
Silicon dioxide	Thermal oxidation, sputtering, anodization, implantation, CVD	Electrical and thermal isolation, masking, encapsulation
Silicon nitride	Plasma CVD	Electr. and thermal isolation, masking, encapsulation

method requires a slowly rotating polycrystalline silicon rod locally melted and recrystallized by a scanning RF heating coil. Very pure silicon results. The silicon is ideal for devices requiring a low doping level to produce, for example, low leakage diodes as required for detectors and power devices.

Routine evaluation of the grown crystalline material involves the measurement of resistivity and crystal perfection. The first is measured with a four-point probe, whereas x-ray or electron beam diffraction helps evaluate the crystal perfection. To prepare wafers from the grown Si boule, first the boule diameter

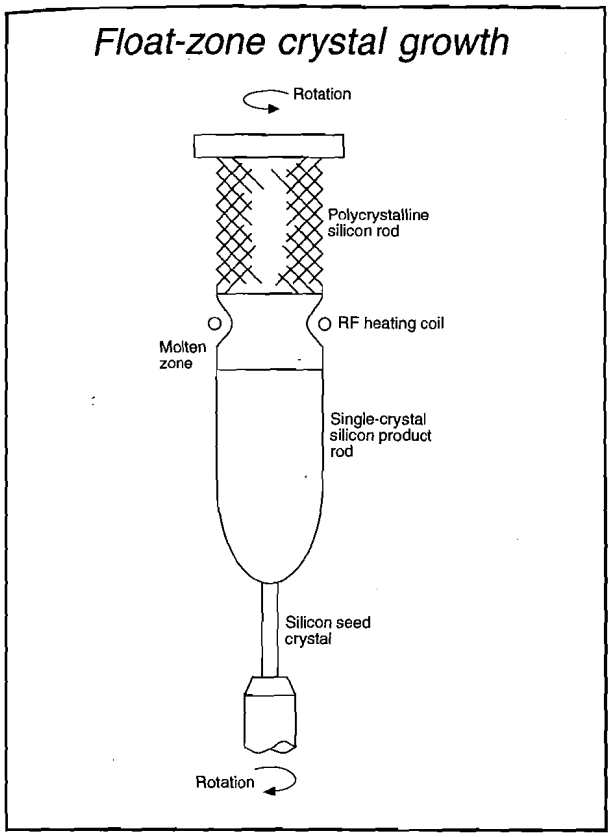

Inset 3.3

is sized by grinding on a lathe; x-rays establish the orientation with an accuracy of ±0.5° (in the very best case). Grinding one or more flats along the length of the ingot follows diameter grinding. Wafer flats help orientation determination and placement of slices in cassettes and fabrication equipment (large primary flat), and they help identify orientation and conductivity type (smaller secondary flat) (see also Figure 4.5). Argon laser markings guide the subsequent slicing. The slices are lapped with a mixture of Al_2O_3 powder in glycerin to produce a wafer with a flatness that is uniform to within 2 μm; the edges are rounded by grinding. Wafer-edge rounding cannot be taken lightly, because it removes micro cracks at the wafer edge, minimizes the source for cracks in silicon chips, makes the wafers more fracture-resistant, increases the mask life, and minimizes resist beading. The edge-rounding process also makes for safer quartz boat loading by increasing the number of transfers of those wafers into quartz boats without chipping.[19] After a damage-removing etch, the wafers are polished and cleaned. The slicing, lapping, edge treatment, damage removal, and polishing result in a material loss of up to 50%.

Typical specifications for a 100-mm (4-in) diameter Si wafer, costing approximately $10, are[8]

- Ø = 100 mm, ±0.5 mm
- Thickness T = 500 μm, ±10 μm
- Primary = flat 30 to 35 mm
- Secondary flat = 16 to 20 mm
- Bow = 40 μm
- Orientation accuracy within 0.5 to 1°

Notice that the thickness control is very limited, which has important consequences for fabricating thin Si membranes. Figure 3.1 illustrates wafer flatness and defect parameters such as bow, warp, chips, etc. Brown provides an excellent further introduction to Si crystal growth.[18]

Doping of Si

Introduction

Elements having one valence electron more or less than Si (with four valence electrons) are used as substitutional donors (n-type)

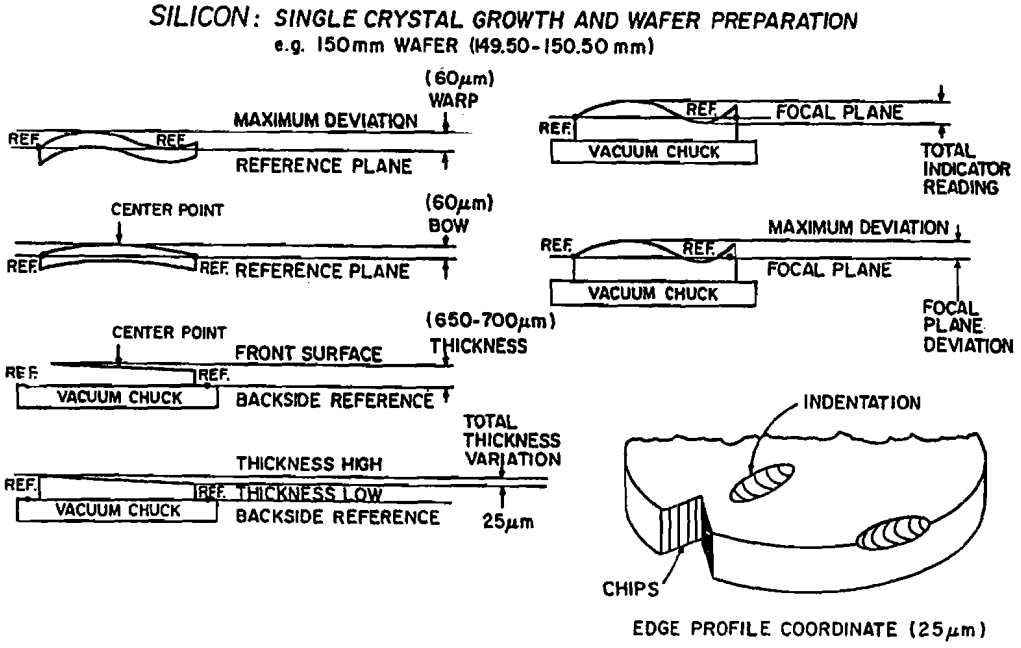

Figure 3.1 Wafer flatness and defect parameters such as bow, warp, and chips. (From A. Wong, "Silicon Micromachining," 1990.[19])

or acceptors (p-type), respectively. Boron (–1), phosphorus (+1), arsenic (+1), and antimony (+1) represent the more commonly used dopant elements. Upon incorporation into the crystal lattice, the dopant either gives up (donor) or receives (acceptor) an electron from the crystal. Fabrication of circuit elements and micromachines requires a method for selective n- or p-type doping of the silicon substrate. The two means of doping Si are diffusion and ion implantation, as shown in Table 3.3.

Conductivity of Semiconductors

In semiconductors, both negative and positive charge carriers contribute to the conductivity. The positive charge carriers (p) are called *holes* because they correspond to an absence of electrons, and μ_p is their mobility. For electrons (e), the mobility is symbolized as μ_e. When both holes and electrons are considered, the conductivity is given as:

$$\sigma = e(n\mu_e + p\mu_p) \tag{3.1}$$

The conductivity σ in $(\Omega\cdot m)^{-1}$ is an intrinsic characteristic of a material and is independent of geometry. It measures the current density for a given electric field. The inverse of the conductivity is the resistivity in $\Omega\cdot m$:

$$\rho = \frac{1}{\sigma} \tag{3.2}$$

Resistivity, in turn, is linked to the resistance R (in Ω) and the geometry of a sample as:

$$R = \rho\frac{L}{A} \tag{3.3}$$

where L is the length and A is the area (Inset 3.4). The resistance R of a thin conductive layer is proportional to the resistivity ρ and inversely proportional to the thickness t. It is convenient to define a sheet resistance, R_s, which is equal to ρ/t. Sheet resistance may be thought of as a material property for conductors that are essentially two-dimensional. For the resistance of a thin deposited conductor layer of length L, thickness t, and width W, we can write:

$$R = \frac{\rho}{t}\frac{L}{W} = R_s\frac{L}{W} \tag{3.4}$$

The ratio L/W is referred to as the number of squares (❑) and is dimensionless. The sheet resistance has the units of ohms, but it is convenient to refer to it as ohms per square (Ω/❑). The resistance of a rectangular thin layer is therefore the sheet resistance times the number of squares (L/W). Sheet resistance of a newly deposited film is typically measured with a four-point probe, an important tool in any IC and MEMS lab. Some background on four-point probe measurements can be found at the University of California, Berkeley, EECS web site (http://argon.eecs.berkeley.edu:8080/~ee143/Four-Point_Probe/). A typical instrument is the SYS-301 from the Signatone Corporation (http://www.signatone.com/4ptprobe.html).

Si Doping by Diffusion

In the past, dopants were typically diffused thermally into the Si substrate in a furnace at temperatures between 950 and 1280°C. For a first approximation, Fick's first and second laws describe the diffusion of dopants in silicon.[20] The dopant flux F is proportional to the concentration gradient as given by Fick's first law:

TABLE 3.3 Characteristics of Two Means of Semiconductor Doping

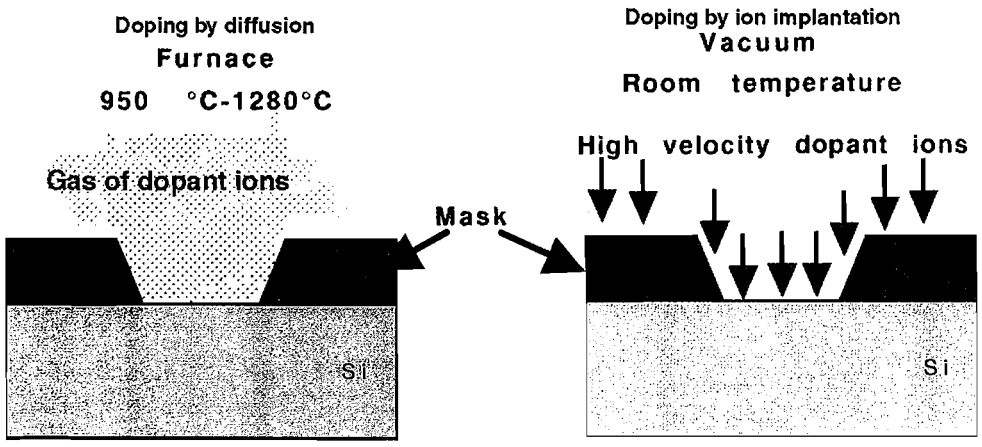

Dopant uniformity and reproducibility	±5% on wafer, ±15% overall	±1% overall
Contamination danger	High	Low
Delineation	Refractory insulators and refractory metals, polysilicon	Refractory and nonrefractory materials, metals
Environment	Furnace	Vacuum
Temperature	High	Low

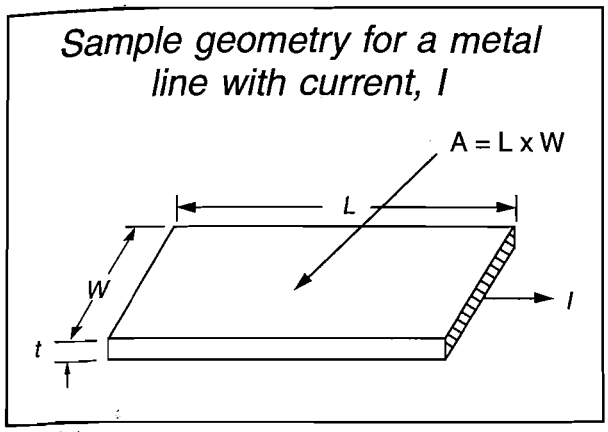

Inset 3.4

$$F = -D\frac{\delta C}{\delta x} \tag{3.5}$$

where D is the diffusion coefficient (D has units of cm²/s) and $\delta C/\delta x$ is the concentration gradient. Equation 3.5 has a negative sign, and $\delta C/\delta x$ is negative for a decrease in the concentration with depth; consequently, the flux into the sample has a positive value.

The flux gradient ($\delta F/\delta x$) is proportional to the change of the concentration with time:

$$\frac{\delta C(x,t)}{\delta t} = -\frac{\delta F}{\delta x} = D\frac{\delta^2 C}{\delta x^2} \tag{3.6}$$

This is also called the *continuity equation* or Fick's second law. The concentration C is generally a function of position x and time t, and in expression 3.6, D is assumed to be constant. The solution to the differential Equation 3.6 depends on the boundary conditions. One common boundary condition is the one in which the surface concentration C_s is constant. This is the case, for example, in gaseous doping of a silicon wafer where the dopant concentration at the Si surface is constant [$C(0,t) = C_s$] while, in the bulk, the concentration remains zero [$C(\infty,t) = 0$] during the whole doping process, resulting in the following relation:

$$C(x,t) = C_s erfc\left(\frac{x}{\sqrt{4Dt}}\right) \tag{3.7}$$

where *erfc* = the complementary error function (see Figure 3.2A)

$\sqrt{Dt}$ = the diffusion length

C_s = the surface concentration of the dopant (in cm^{-3})

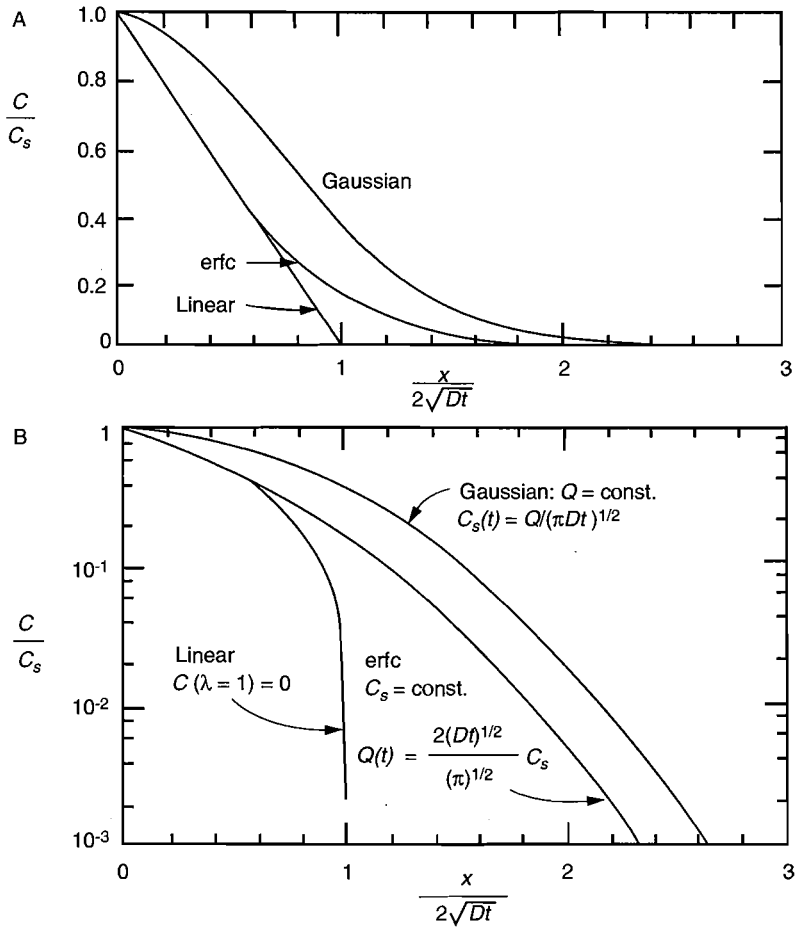

Figure 3.2 Diffusion functions: normalized concentration vs. normalized distance. (A) Gaussian and erfc as a function of $x/(2\sqrt{Dt})$. (B) Semi-log plot of various diffusion functions as a function of $x/(2\sqrt{Dt})$.

One typically also introduces a parameter $\lambda = \sqrt{4Dt}$, that is, the characteristic diffusion length. This quantity measures the distance where the concentration of the diffusing atoms drops down to zero in the case of a linear concentration gradient (Figure 3.2A). Generally speaking, this same boundary condition applies for predeposition of dopant atoms into semiconductor substrates. Typical dopant sources used are $POCl_3$ (liquid), BN_3 (solid), and PH_3 (gas) or B_2H_6 (gas). The temperature of the substrates is usually kept between 800 and 1200°C, and the surface concentration C_s of the impurities during predeposition is constant. The total amount of dopant atoms diffusing from an outside source into the substrate, Q, is given by integration of Equation 3.7:

$$Q(t) = \int_0^\infty C_s erfc\left(\frac{x}{\sqrt{4Dt}}\right)dx = \frac{2\sqrt{Dt}}{\sqrt{\pi}}C_s \qquad (3.8)$$

The concentration profile of the doping impurities is linear up to a distance of 0.6 λ (see Figure 3.2B).

Another boundary condition applies when the dopant concentration at the silicon surface is limited; in other words, the diffusing amount Q is constant and $C(\infty,t) = 0$. In this case. the resulting dopant concentration profile is Gaussian instead of an *erfc* function (Figure 3.2A). In this boundary condition, the surface dopant concentration falls as the material supply is depleted. The solution of Equation 3.6 in this instance is given as:

$$C(x,t) = \frac{Q}{\sqrt{\pi Dt}}\exp\left(-\frac{x^2}{4Dt}\right) \qquad (3.9)$$

At the surface, $x = 0$, and Equation 3.9 equals:

$$C_s = C(0,t) = \frac{Q}{\sqrt{\pi Dt}} \qquad (3.10)$$

(See Figure 3.2B.) In other words, the surface concentration changes as $(Dt)^{-1/2}$. This type of boundary condition is typical for drive-in diffusion. The dopants introduced in the substrate by a predeposition step are redistributed deeper into the substrate to lower the concentrations by such a drive-in step.

The D in the above equations is the dopant diffusivity and is given by:

$$D = D_0(T_0)\exp\left(-\frac{E_a}{kT}\right) \qquad (3.11)$$

with E_a the activation energy with a value (typically 0.5 to 1.5 eV) that depends on the transport mechanism. The diffusion coefficient, D_0, is merely a constant for a given reaction and concentration. Dopant atoms take on several different ionization states and diffuse by as many different mechanisms. The effective diffusion coefficient is actually the sum of the diffusivities of each species, which in turn are a function of temperature and dopant concentration. Hence, actual dopant concentration profiles deviate from the simple first-order functions given above.

The dopant diffusivities of phosphorus, arsenic, and boron in silicon at 1100°C typically are 2×10^{-13}, 1×10^{-13}, and 1×10^{-13} cm²/s, respectively. Below the intrinsic carrier concentration (~5×10^{18} cm^{-3} for Si at 1000°C), D is independent of the concentration. Above the intrinsic concentration, the diffusion increases with carrier concentration and generally follows a power law due to the diffusion mechanism becoming point defect (i.e., vacancies and interstitials) assisted.

One can make use of calibration charts to determine a more practical value of the characteristic diffusion length λ (see above) typically referred to as the junction depth λ_p, based on:

$$\lambda_p = k\sqrt{D_s t} \qquad (3.12)$$

where k represents a coefficient that depends on the diffusivity regime and can take a value from 1.6 to 0.87, D_s is the surface diffusivity and is a function of the dopant material and the temperature, and t is the diffusion time.[20] It is important to remember that the concentration profile of the dopant in the semiconductor never changes abruptly, as this would imply a zero or infinite flux, so diffusion always spreads impurities gradually around the edges of any mask.

Typical diffusion furnaces may be obtained from the Sizary Company (http://www.crystec.com/sizprome.htm) and Sony Semiconductor (http://www.foundry.sony.com/diffusio.htm).

Doping by Implantation

The principal method of Si doping today centers on high-energy ion beam implantation. Implantation offers the advantage of being able to place any ion at various depths in the sample, independent of the thermodynamics of diffusion and problems with solid solubility and precipitation. Ion beams produce crystal damage* that can reduce electrical conductivity. Most of this damage can be eliminated, though, by annealing at 700 to 1000°C. The anneal temperature is high enough for Si interstitial atoms to recombine with vacant lattice sites and for the dopant atoms to move to substitutional lattice sites where they are electrically active. The combination of excellent spatial and dose control, as well as ease of manufacture, has led to widespread use of ion implantation.

A beam of energetic ions "implants" charged dopants atoms into the Si substrate. Depth and dopant concentration are controlled by the acceleration energy and the beam current. The implanted dopant atoms enter unmasked regions in the silicon lattice at high velocity. The stopping mechanism of the ions involves nuclear collisions at low energy and electronic interactions at high energy. Photolithography is used to mask the regions of the device where doping is not desired.

The jargon associated with ion implantation includes[20]

- Projected range R_p; i.e., average distance traveled by ions parallel to the beam

* The implant energy, between 30 and 100 kiloelectron volts (keV), is thousands of times the silicon bond energy.

- Projected straggle, ΔR_p; i.e., fluctuation in the projected range
- Lateral straggle, $\Delta R//$; i.e., fluctuation in the final rest position, perpendicular to the beam
- Peak concentration, N_p; i.e., concentration of implanted ions at R_p

In the absence of crystal orientation effects, the concentration profile, to a first-order approximation, is Gaussian:

$$N_i(x) = \frac{Q_i}{(2\pi)^{\frac{1}{2}}\Delta R_p} \exp\left[-\frac{1}{2}\left(\frac{x - R_p}{\Delta R_p}\right)^2\right] \qquad (3.13)$$

where N_i = implanted atoms
Q_i = total implanted dose (ions/cm^2)

The range is determined by the acceleration energy, the ion mass, and the stopping power of the material. Orientation of the substrate surface away from perpendicular to the beam prevents channeling, which can occur along crystal planes, ensuring better reproducibility of R_p. Ion channeling leads to an exponential tail in the concentration vs. depth profile. This tail is due to the crystal lattice and is not observed in an amorphous material. The dose Q_i is determined by the charge per ion, zq; the implanted area, A; and the charge per unit time (current) arriving at the substrate. In other words:

$$\int i dt = Q_i \qquad (3.14)$$

$$\text{and } \frac{Q_i}{[zqA]} = \text{Dose(atom/cm}^2\text{)}$$

The technique is now very commonly used, with penetration depths in silicon of As, P, and B typically being 0.5, 1, and 2 μm at 1000 keV.

Thermal annealing at temperatures above 900°C is required to remove defects from the silicon lattice and to activate the implanted impurities. For the newest and future generations of CMOS devices that require highly doped, abrupt, and shallow profiles (junction depths less than 30 nm!), the dopant diffusion step during annealing must be minimized. Technologies studied in this context are ultra-low-temperature processing and rapid thermal annealing.[21] For deep diffusions (>1 μm), implantation is used to create a dose of dopants, and thermal diffusion is used to drive in the dopant. For a recent update on defects and diffusion in Si, see *MRS Bulletin*, June 2000, Volume 25, Number 6.

Ion beams can implant enough material to actually form new materials (i.e., oxides and nitrides), some of which show improved wear and strength characteristics. Ion implanters may be purchased from Varian Semiconductor (http://www.vsea.com/) and Eaton Corporation (http://www.eaton.com/). This equipment is very expensive, and usually service providers are used instead.

Oxidation of Silicon

Kinetics

Silicon dioxide growth involves the heating of a silicon wafer in a stream of steam at 1 atm or in wet or dry oxygen/nitrogen mixtures (Inset 3.5) at elevated temperatures (between 600 and 1250°C). Silicon readily oxidizes, even at room temperature, forming a thin native oxide approximately 20 Å thick. The high temperature aids diffusion of oxidant through the surface oxide layer to the silicon interface to form thick oxides quickly:

$$Si + 2H_2O \rightarrow SiO_2 + H_2 \text{ (wet)} \qquad \text{Reaction 3.1}$$

$$Si + O_2 \rightarrow SiO_2\text{(dry)} \qquad \text{Reaction 3.2}$$

Another gas phase oxidation method of Si is the pyrogenic method (Inset 3.5). Besides oxygen and nitrogen, the gas also contains hydrogen in this case. The ratio of silicon thickness converted (Inset 3.6), X_S, to resulting oxide thickness, X_{OX}, is proportional to their respective densities:

$$X_s = 0.46X_{ox} \qquad (3.15)$$

When 10,000 Å of oxide has grown, 4600 Å of Si will be consumed; in other words, the amount of silicon consumed is 46% of the final oxide thickness. This relationship is important for calculating step heights that form in silicon microstructures.

All gas phase oxidation processes involve three steps in series: gas phase transport of oxidant to the surface (F_1), diffusion through the existing oxide (F_2), and the oxidation reaction itself (F_3). Equilibrating the fluxes $F_1 = F_2 = F_3$ in Figure 3.3 yields the concentration of oxidant at the interface oxide/silicon, C_i:

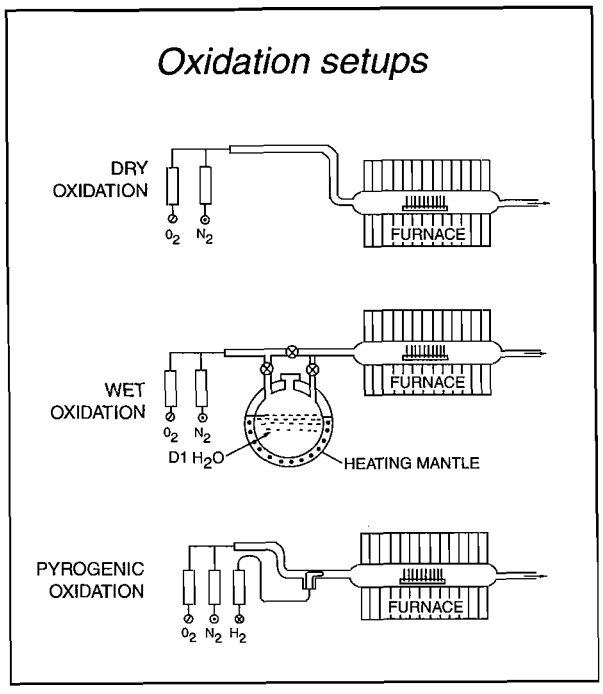

Inset 3.5

is why, in such devices, SiO_2 is often topped off with the excellent ionic barrier material Si_3N_4. The use of SiO_2 as a diffusion mask often stems from convenience; SiO_2 is easy to grow, whereas Si_3N_4 cannot be put directly onto Si.

The quality of silicon dioxide depends heavily on its growth method. Dry oxidation at high temperature (between 900 and 1150°C) in pure oxygen produces a better quality oxide than steam oxidation. Such a thermal oxide is stoichiometric, has a high density, and is basically pinhole free. Wet oxidation in steam occurs much faster but produces a lesser quality oxide, while water causes a loosening effect on the SiO_2, making it more prone to impurity diffusion. Both types of oxidation are carried out in a quartz tube. Oxide thicknesses of a few tenths of a micron are used most frequently, with 1 to 2 μm being the upper limit for conventional thermal oxides. Addition of chlorine-containing chemicals during oxidation increases the dielectric breakdown strength and the rate of oxidation and improves the threshold voltage of many electronic devices;[33] however, too high concentrations of halogens at high temperatures can pit the silicon surface. The influence of chlorine, hydrogen, and other gases on the SiO_2 growth rate and the resulting interface and oxide quality has been a fertile research field, a short summary of which can be found in Fair.[24] It should be noted that, except in the IC Industry, the electronic quality of the Si/SiO_2 interface as expressed through low concentrations of interface trap states, low fixed oxide surface charges, low bulk oxide trapped charges, and mobile charges (Inset 3.7[20]) (impurity ions such as Li^+, Na^+, K^+) is of no importance in micromachining. In micromachining, the oxide only proves useful as a structural element, a sacrificial layer, or a dielectric in a passive device. One notable exception is the aforementioned ISFET, where the electronic properties of the gate oxide are key to its functioning; a perfect oxide and oxide/semiconductor interface hold as much importance in this case as it does in the IC industry.

In conclusion, thermal oxidation involving the consumption of a surface results in excellent adhesion and good electrical and mechanical properties. It is an excellent technique when available.

In Table 3.5, we review some of the more significant properties of thermally grown SiO_2.

Physical Vapor Deposition

Introduction

Many different kinds of thin films in ICs and micromachines are deposited by evaporation and sputtering, both of which are examples of PVD. PVD reactors may use solid, liquid, or vapor as raw material in a variety of source configurations. Other PVD techniques, very useful in the deposition of complex compound materials, are molecular beam epitaxy (MBE) and laser ablation deposition. Ion plating and cluster deposition are based on a

Location of oxide charges in thermally oxidized silicon structures

(From I. Brodie and J. J. Muray, *The Physics of Microfabrication,* Plenum Press, New York, 1989. With permission.)

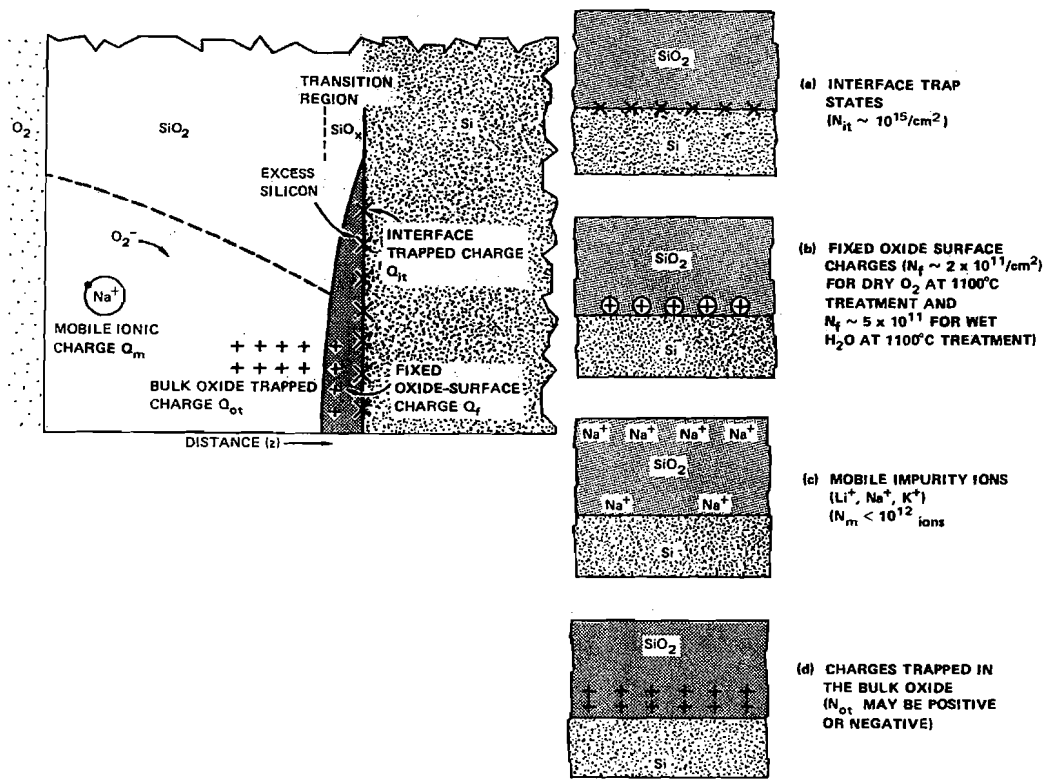

Inset 3.7

TABLE 3.5 Properties of Thermal SiO_2

Property	Value
Density (g/cm³)	2.24–2.27 (dry) and 2.18–2.20 (wet)
Dielectric constant	3.9
Dielectric strength (V/cm)	2×10^6(dry) and 3×10^6 (wet)
Energy gap (eV)	~8
Etch rate in buffered HF (Å/min)	1000
Infrared absorption peak (μm)	9.3
Melting point (°C)	~1700
Molecular weight	60.08
Molecules/cm³	2.3×10^{22}
Refractive index	1.46
Resistivity at 25°C (Ω-cm)	3×10^{15} (dry) $3–5 \times 10^{15}$ (wet)
Specific heat (J/g° C)	1.0
Stress in film on Si (dyne/cm²)	$2–4 \times 10^8$ (compressive)
Thermal conductivity (W/cm°C)	0.014
Thermal conductivity (W/cmK)	0.014
Thermal linear expansion coefficient (°C⁻¹)	5×10^{-7} (0.5 ppm/°C)

combination of evaporation and plasma ionization and offer some of the advantages inherent to both techniques. The key distinguishing attribute to a PVD reactor is that the deposition of the material onto the substrate is a line-of-site impingement type. At the low pressures employed in a PVD reactor, the vaporized material encounters few intermolecular collisions while traveling to the substrate. Modeling of deposition rates is consequently a relatively straightforward exercise in geometry.

Thermal Evaporation

Thermal evaporation represents one of the oldest of thin film deposition techniques. Evaporation is based on the boiling off (or sublimating) of a heated material onto a substrate in a vacuum. From thermodynamic considerations, the number of molecules leaving a unit area of evaporant per second or flux F is given by:

$$F = N_0 \exp -\left(\frac{\Phi_e}{kT}\right) \tag{3.22}$$

where N_0 is a slowly varying function of temperature (T) and Φ_e is the activation energy (in eV) required to evaporate one molecule of the material. The activation energy for evaporation is related to the enthalpy of formation of the evaporant, H, as $H = \Phi_e \times e \times N$ (Avogadro's number) J/mol.

Table 3.6 suggests the need for a good vacuum during evaporation; even at a pressure of 10^{-5} Torr, 4.4 contaminating monolayers per second will redeposit on the substrate.[20] For reference purposes, the number of atoms per unit area corresponding to a monolayer for a metal is about 10^{15} atoms/cm². Moreover, to avoid reactions at the source (e.g., oxide impurities being formed), the oxygen partial pressure needs to be less than 10^{-8} Torr.

TABLE 3.6 Kinetic Data for Air as a Function of Pressure

Pressure (Torr)	Mean free path (cm)	Number impingement rate (S^{-1}, cm^{-2})	Monolayer impingement rate (s^{-1})
10^1	0.5	3.8×10^{18}	4400
10^{-4}	51	3.8×10^{16}	44
10^{-5}	510	3.8×10^{15}	4.4
10^{-7}	5.1×10^4	3.8×10^{13}	4.4×10^{-2}
10^{-9}	5.1×10^6	3.8×10^{11}	4.4×10^{-4}

Source: I. Brodie and J. J. Muray, *The Physics of Microfabrication*, Plenum Press, New York, 1982.[20] Reprinted with permission.

In laboratory settings, a metal is usually evaporated by passing a high current through a highly refractory metal containment structure (e.g., a tungsten boat or filament). This method is called "resistive heating" (Figure 3.5A). Resistive evaporation is simple but easily spreads contaminants that are present in the filament, and the small size of the filament limits the thickness of the deposited film. In industrial applications, resistive heating has been surpassed by electron-beam (e-beam) and RF induction evaporation. In the e-beam mode of operation, a high-intensity electron beam gun (3 to 20 keV) is focused on the target material that is placed in a recess in a water-cooled copper hearth. As shown in Figure 3.5B, the electron beam is magnetically directed onto the evaporant, which melts locally. In this manner, the metal forms its own crucible, and the contact with the hearth is too cool for chemical reactions, resulting in fewer source-contamination problems than in the case of resistive heating. E-beam evaporation not only results in higher quality films, it also provides a higher deposition rate (50–500 nm/min). Two disadvantages of e-beam evaporation are that the process might induce x-ray damage and possibly even some ion damage to the substrate (at voltages > 10 kV, the incident electron beam will cause x-ray emission) and that the deposition equipment is more complex. X-ray damage may be avoided by using a focused, high-power laser beam instead of an electron beam. However, this technique has not yet penetrated commercial applications. In RF induction heating, a water-cooled RF coupling coil surrounds a crucible with the material to be evaporated. Since about two-thirds of the RF energy is absorbed within one skin depth of the surface, the frequency of the RF supply must decrease as the size of the evaporant charge increases. With a charge of a few grams of evaporant, frequencies of several hundred kilohertz are sufficient.

In Table 3.7, we compare the different heat sources available for thermal evaporation. The substances used most frequently for thin-film formation by evaporation are elements or simple compounds whose vapor pressures range from 1 to 10^{-2} Torr in

TABLE 3.7 Comparison of Heat Sources for Evaporation

Heat sources	Advantages	Disadvantages
Resistance	No radiation	Contamination
e-beam	Low contamination	Radiation
RF	No radiation	Contamination
Laser	No radiation, low contamination	Expensive

mines proper operation, material purity is a priority consideration. In chemical sensors, the surface purity of films is more important than the bulk resistivity (a criterion often used to evaluate IC films). As we just learned, evaporators emit material from a point source (e.g., a small tungsten filament), resulting in shadowing and sometimes causing problems with deposition, especially on high-aspect structures. Difficulties also arise for large areas where highly homogeneous films are required, unless special setups are chosen. A different problem to overcome arises from the source materials decomposing at high evaporation temperatures. While this risk does not exist when evaporating pure elements, it becomes a problem in the evaporation of compounds and substance mixtures. The e-beam heating systems have an advantage here, since only a small part of the metal source evaporates. The initial evaporant stream is richer in the higher-vapor-pressure component; however, the melt depletes that constituent locally, and eventually an equilibrium rate is established. The best way to deposit complex metal alloys is then to e-beam evaporate the metallic elements from different sources as modern quartz-crystal deposition rate monitors enable excellent control in alloy composition. To form oxides of the deposited metals, evaporation is performed in a low-pressure oxygen atmosphere. This process is known as *reactive evaporation*. The oxygen supply comes from a jet directed at the substrate during deposition. To obtain the correct stoichiometry, the deposition needs to take place on a heated substrate.

Evaporated thin films are usually under tensile stress, and the higher the material's melting point the higher the stress. Tungsten and nickel, for example, can have stress in excess of 500 MPa, which may lead to curling or peeling.[37] Raising the temperature of the substrate tends to lower the internal stresses in the thin film (see also Chapter 5).

Sputtering

During sputtering, the target (a disc of the material to be deposited), at a high negative potential, is bombarded with positive argon ions (other inert gases such as Xe can be used as well) created in a plasma (also glow discharge). The target material is sputtered away mainly as neutral atoms by momentum transfer and ejected surface atoms are deposited (condensed) onto the substrate placed on the anode (Figure 2.8). Sputtering is preferred over evaporation in many applications due to a wider choice of materials to work with, better step coverage, and better adhesion to the substrate. Actually, sputtering is employed in laboratories and production settings, whereas evaporation mainly remains a laboratory technique. Other reasons to choose sputtering over evaporation can be concluded from a comparison of the two techniques in Table 3.8.

TABLE 3.8 Comparison of Evaporation and Sputtering Technology

	Evaporation	Sputtering
Rate	Thousand atomic layers per second (e.g., 0.5 μm/min for Al)	One atomic layer per second
Choice of materials	Limited	Almost unlimited
Purity	Better (no gas inclusions, very high vacuum)	Possibility of incorporating impurities (low-medium vacuum range)
Substrate heating	Very low	Unless magnetron is used substrate heating can be substantial
Surface damage	Very low, with e-beam x-ray damage is possible	Ionic bombardment damage
In situ cleaning	Not an option	Easily done with a sputter etch
Alloy compositions, stochiometry	Little or no control	Alloy composition can be tightly controlled
X-ray damage	Only with e-beam evaporation	Radiation and particle damage is possible
Changes in source material	Easy	Expensive
Decomposition of material	High	Low
Scaling-up	Difficult	Good
Uniformity	Difficult	Easy over large areas
Capital equipment	Low cost	More expensive
Number of depositions	Only one deposition per charge	Many depositions can be carried out per target
Thickness control	Not easy to control	Several controls possible
Adhesion	Often poor	Excellent
Shadowing effect	Large	Small
Film properties (e.g., grain size and step coverage)	Difficult to control	Control by bias, pressure, substrate heat

As most aspects pertaining to the physics and chemistries of dc and RF plasmas were discussed in Chapter 2, we will only amplify the material here as it applies to deposition. During ion bombardment, the source is not heated to high temperature, and the vapor pressure of the source is not a consideration as it is in vacuum-evaporation. The amount of material, W, sputtered from the cathode is inversely proportional to the gas pressure, P_T, and the anode-cathode distance, d:[20]

$$W = \frac{kVi}{P_T d} \tag{3.30}$$

where V = working voltage
i = discharge current
k = a proportionality constant

Other energetic particles, such as secondary electrons, secondary ions and photons, and x-rays, are created at the target and can be incorporated in the growing film and/or influence its properties through heating, radiation, or chemical reactions. The sputter yield, S, stands for the number of atoms removed per incident ion and is a function of the bombarding species, the ion energy of the bombarding species, the target material, the incident angle of the bombarding species, and its electronic charge. Deposition rate is roughly proportional to yield for a given plasma energy. Some yield figures for commonly used metals are tabulated in Table 3.9.[15]

TABLE 3.9 Sputter Yields of Several Commonly Used Materials with 500 eV Argon

Element	Symbol	Sputter yield
Aluminum	Al	1.05
Chrome	Cr	1.18
Gold	Au	2.4
Nickel	Ni	1.33
Platinum	Pt	1.4
Titanium	Ti	0.51

Source: J. L. Vossen and W. Kern, *Thin Film Processes*, Academic Press, New York, 1978.[15] Reprinted with permission.

A typical sputter yield as a function of ion energy was shown already in Figure 2.11.[20] In the low-energy region, the yield increases rapidly from a threshold energy. The sputter threshold, usually in the range of 10 to 130 eV, is essentially independent of the bombarding ion species used and equals about four times the activation energy for evaporation. This threshold voltage decreases with increasing atomic number within each group of the periodic table. Above a few hundred volts, a changeover region takes hold. Its value depends on the ion species and target used, but, after its occurrence, the sputter yield increases more slowly. Ion energies in the range of 0.5 to 3 kV are typically used for sputter deposition, as nuclear collisions are predominant in this range. In this region, the sputter yields range from 0.1 to 20 atoms per ion, and the yield of most metals is about 1 (see Table 3.9). An ion can penetrate only up to a certain depth into the target and still effect a recoil collision that can reach the surface with sufficient energy to eject atoms (e.g., 1 nm/kV penetration for argon ions in copper).

Consequently, at ion bombardment energies in the range of 10 keV to 1 MeV, the sputter yield reaches a maximum and then gradually declines in value as a result of deep ion implantation. Average ejection energies of ions from the target range between 10 and 100 eV. At those energies, the incident ion can penetrate a substrate one to two atomic layers into the surface on which it lands. As a result, the adhesion of sputtered films is superior to films deposited by other methods.[38] Although sputtering is basically a low-temperature process, considerable amounts of energy are dissipated at the target surface. To liberate one atom requires 100 to 1000 times the activation energy needed for evaporation, limiting useful sputtering rates to about one atomic layer per second (1000 times less than evaporation from a source operating at 10^{-1} Torr). The target needs water cooling, as most of the energy, estimated at about 75%, dissipates into it, and excessive heating might result. Only one percent of the remaining energy goes into sputtering, and the rest is dissipated by secondary electrons that bombard and heat the substrate. Figure 2.8 exemplifies a typical sputtering setup. Sputtering systems often have a load-lock connected to the sputtering chamber used for loading and unloading the substrates. With the use of a load-lock system, the sputtering station can be kept under continuous high vacuum; the target and chamber can be kept free of contamination from gaseous atmospheric components. Instead of pumping the large sputtering chamber, only the small load-lock chamber is pumped, resulting in a significant shorter cycle time. To prevent sputtering of the structural elements of the cathode assembly, a shield of metal at anode potential is placed around all of the surfaces to be protected at a distance less than that of the dark space at the cathode in Figure 3.7.[38] No discharge will take place between two surfaces that have a separation less than the Crookes cathode dark space (see Chapter 2).

Crucial to the formation of a sustained dc plasma, as discussed in Chapter 2, is the production of ionizing collisions

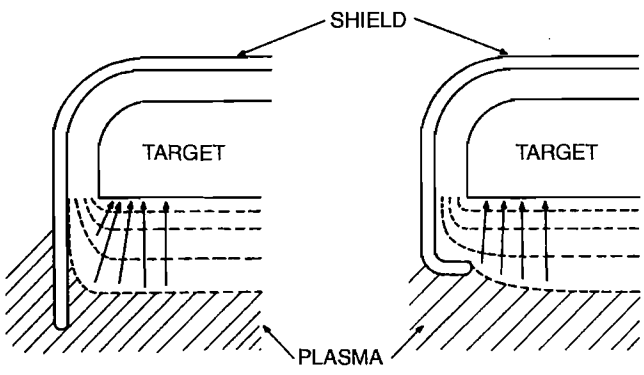

Figure 3.7 Sputtering: use of cathode shield. (Left) Reducing rim effect by extending cathode shield. (Right) Reducing rim effect by wrapping shield around the cathode. (From L. I. Maissel and R. Glang, Eds., *Handbook of Thin Film Technology*, McGraw-Hill, New York, 1970.[38] Reprinted with permission.)

between secondary electrons released from the cathode and the gas in the sputtering chamber. In effect, this requires a relatively high working pressure of greater than 1×10^{-2} Torr. However, if the pressure is too high, significant numbers of the sputtered atoms cannot pass through the sputtering gas and are reflected back to the cathode by collisions. At 10^{-1} Torr, the mean free path of the sputtered metal atoms is about 1 mm, which is near the practical limit. Because of the multiple collisions of the metal atoms in the path between the cathode and anode, the metal atoms arrive at the anode at random incident angles. This leads to a better step coverage as compared with evaporation. Furthermore, as the sputtering target is very broad as compared with an evaporation point source, evidence of shadowing decreases drastically. Sputtering at low gas pressure leads to improved film adhesion, because the sputtered atoms have a higher energy. Reduced pressure also reduces contamination of the film by trapped gas molecules, resulting in films of higher density and purity. The higher material density causes a slower chemical etch of the deposited film. For conductors, a dc sputtering setup can be used. Insulating materials require an RF power supply. Before sputter deposition, the substrate may be sputter etched by connecting it to the negative pole of the power supply. Sputter cleaning further promotes adhesion of subsequent metallizations. *In situ* cleaning can also be done efficiently with an ion gun. As in dry etching, the plasma can be confined and densified by using electron cyclotron resonance (ECR) in a planar or cylindrical magnetron or an S-gun using a conical magnetron, which produces higher deposition rates than evaporation produced by electron beam (e-beam) or RF induction. Higher ion densities permit higher sputter rates. In a magnetron sputtering apparatus, the crossed electric and magnetic fields contain the electrons and force them into long, helical paths, thus increasing the probability of an ionizing collision with an argon atom. Furthermore, secondary electrons emitted by the cathode due to ion bombardment are bent by the crossed fields and are collected by ground shields. This eliminates the secondary electron bombardment of the substrates, which is one of the main sources of unplanned substrate heating. The deposition rate reaches hundreds of angstrom per minute. For some materials, such as aluminum, the deposition rate can be as high as 1 μm/min. Magnetron sputter enhancement can be used in high-frequency sputtering systems as well as in dc sputtering systems. The substrate is also often heated to promote film adhesion and reduce film stress. Stress levels vary from compressive at low pressures (0.1–1 Pa) to tensile at high pressures (1–10 Pa). The transition regime between compressive and tensile is often sharp (over a few tenths of Pa), making the crossover (an ideal point for zero-stress deposition) difficult to control.[37] In general, it is preferable to have ions strike the substrate while growing a film. The plasma ions add energy to the film and keep the surface atoms mobile enough to fill virtually every void. The influence of a plasma on a depositing film is considered in more detail in the section on *Plasma-Enhanced CVD*, page 148.

Sputtering often is carried out in the presence of a reactive gas, ensuring control or modification of the properties of the deposited film in so-called *reactive sputtering*. A sensor material produced this way is IrO_x, a low-impedance pH sensing material arrived at by sputtering from a pure Ir target with argon ions in the presence of oxygen.[39] The exact mechanism for compound formation in reactive sputtering still eludes researchers. It is conjectured that, at low pressures, the reaction takes place at the substrate as the film is being deposited. At high pressure, the reaction is believed to occur at the cathode, with the compound being transported to the substrate. Composite films can also be made by co-sputtering or by sputtering from a single composite target. Since the various elements in a target have different sputtering rates and sticking probabilities, the composition of the target can differ from that on the substrate. The decomposition is less significant than in evaporation and can be compensated automatically by the changes in target surface composition resulting from preferential sputtering of one of the components until a new balance is reached. High substrate temperatures are needed to obtain the right composition and to promote adhesion.

Nowadays, sputtering equipment applies films to compact discs, computer disks, large-area active-matrix liquid crystal displays, and magneto-optic disks.[40] Also, bearing gears, saw blades, and so on can be coated with a number of hard, wear-resistant coatings such as TiN, TiC, TiAlN, NbN, CrN, TiNbN, and CrAlN.[41] Commercial in-line sputtering equipment is available, enabling, in a series of evacuated chambers and load locks, depositions of insulators such as SiO_2, Si_3N_4, Ta_2O_5, metals, and semiconductors such as indium tin oxide (ITO) on substrate with sizes of 830×1500 mm. In one particular setup, one can actually perform continuous deposition (Inset 3.8) on substrates, including foils and fabrics. In a high-vacuum chamber, the substrate is unwound and passes over the cathode cylinder where thin layers of target material are deposited. The substrate is continuously rewound on the other side of the deposition site. The sputter target is a long cylinder, and reactive and nonreactive processes are available.[42] Innovations like these might help revive the potential of micromachined chemical sensors for which Si batch processes are often too expensive. When manufacturing microfabricated chemical sensors, one often competes with continuous fabrication processes (e.g., continuous printing of glucose sensor paper strips), and classical Si micromachining cannot beat the cost advantages these offer. A process as described here, complemented by continuous lithography, might enable chemical microsensor fabrication at an acceptable cost (see Example 3.3).

The most negative aspects of sputtering are its complexity as compared with an evaporation process, the excessive substrate heating due to secondary electron bombardment, and, finally, the slow deposition rate. In a regular sputtering process, the rate is one atomic layer per second vs. thousand atomic layers per second available from a typical evaporation source at a vapor pressure of 10^{-1} Torr. Controls in a sputtering setup include argon pressure, flow rate, substrate temperature, sputter power, bias voltage, and electrode distance.

Molecular Beam Epitaxy

Epitaxial techniques arrange atoms in single-crystal fashion upon a crystalline substrate acting as a seed crystal so that the

ing, and low-temperature thin film formation. Cluster ion beam processing is now expanding into new industrial fields, which are presently limited by the available atomic and molecular ion beam processes.

With the wide variety of selective layers needed in chemical sensors and the frequent need for low-temperature deposition of thick, well adhering layers, ion plating, laser sputtering, and cluster beam technology seem destined to play a more crucial role in chemical sensor development in the future. Also, building devices from atomic constituents (bottom-up approach), with proximal probes for example (see Chapters 1 and 7), is too time consuming when performed one atom at the time. To speed up the process, massive parallelism is required; for example, by using an army of coordinated proximal probes. Cluster beam technology better enables nanomachining, since the size of the building blocks lends itself to building components faster. Epion (http://www.epion.com/) is an example of a company selling ion cluster beam equipment, and their units feature surface smoothing to less than 3 Å, surface cleaning, and high yield sputtering.

Chemical Vapor Deposition

Introduction

During CVD, the constituents of a vapor phase, often diluted with an inert carrier gas, react at a hot surface (typically higher than 300°C) to deposit a solid film. In CVD, the diffusive-convective transport to the substrate involves intermolecular collisions. Mass and heat transfer modeling of deposition rates is consequently much more complex than in PVD. In the reaction chamber, the reactants are adsorbed on the heated substrate surface, and the adatoms undergo migration and film-forming reactions. Gaseous by-products are desorbed and removed from the reaction chamber. The reactions forming a solid material do not always occur on or close to the heated substrate (heterogeneous reactions) but can also occur in the gas phase (homogeneous reactions). As homogeneous reactions led to gas phase cluster deposition and result in poor adhesion, low density, and high-defect films, heterogeneous reactions are preferred. The slowest of any of the CVD steps mentioned, the gas phase or surface process determines the rate of deposition. The sample surface chemistry, its temperature, and thermodynamics determine the compounds deposited. The most favorable end product of the physical and chemical interactions on the substrate surface is a stoichiometric-correct film. Several activation barriers need to be surmounted to arrive at this end product. Some energy source, such as thermal, photon, or ion bombardment, is required to achieve this.

The CVD method is very versatile and works at low or atmospheric pressure and at relatively low temperatures. Amorphous, polycrystalline, epitaxial, and uniaxially oriented polycrystalline layers can be deposited with a high degree of purity, control, and economy. CVD is used extensively in the semiconductor industry and has played an important role in transistor miniaturization by introducing very thin film deposition of silicon. Most recently, CVD copper and low-dielectric insulators ($\varepsilon < 3$) also have become important CVD applications. CVD embodies the principal building technique in surface micromachining (Chapter 5). In the case of a CVD reactor, the diffusive-convective transport to the substrate involves many intermolecular collisions. Accordingly, mass and heat transfer modeling of deposition rates becomes more complex. When a molecule has reached the surface, the required reaction analysis is the same, regardless of deposition method. The molecular phenomena at the surface to be considered include sticking coefficient, surface adsorption, surface diffusion, surface reaction, desorption, and film or crystal growth.

Reaction Mechanisms

Figure 3.13 schematically illustrates the various transport and reaction processes underlying CVD:[48]

- Mass transport of reactant and diluent gases (if present) in the bulk gas flow region from the reactor inlet to the deposition zone
- Gas phase reactions (homogeneous) leading to film precursors and by-products (often unselective and undesirable)

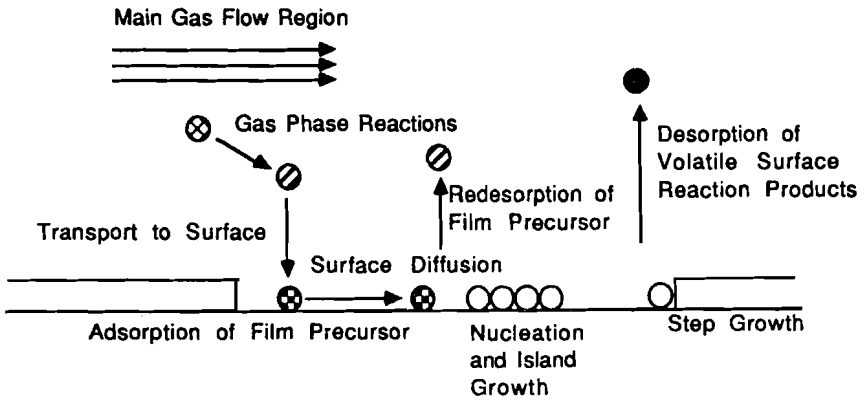

Figure 3.13 Schematic of transport and reaction processes underlying CVD. (From K. F. Jensen in *Microelectronics Processing: Chemical Engineering Aspects*, Hess. D. W., Jensen, K. F. (Eds.), Advances in Chemistry Series 221, American Chemical Society, Washington, DC, 1989.[48] Copyright 1989 American Chemical Society. Reprinted with permission.)

- Mass transport of film precursors and reactants to the growth surface
- Adsorption of film precursors and reactants on the growth surface
- Surface reactions (heterogeneous) of adatoms occurring selectively on the heated surface
- Surface migration of film formers to the growth sites
- Incorporation of film constituents into the growing film; that is, nucleation (island formation)
- Desorption of by-products of the surface reactions
- Mass transport of by-products in the bulk gas flow region away from the deposition zone toward the reactor exit

Energy to drive reactions can be supplied by several methods (e.g., thermal, photons, or electrons), but thermal energy is the most widely used. In the case of a thermally driven CVD reaction, a temperature gradient is imposed on the reactor, the gas phase species (e.g., SiH_4) forms in a hot region, and the equilibrium shifts toward the desired solid (e.g., Si) in a slightly colder region. Either the gas phase or the surface processes can determine rate.

The transport in the gas phase takes place through diffusion proportional to the diffusivity of the gas, D, and the concentration gradient across the boundary layer that separates the bulk flow (source) and substrate surface (sink). The flux of depositing material is given by Equation 3.5 (Fick's first law). The boundary layer thickness, $\delta(x)$, as a function of distance along the substrate, x (see Figure 3.14), can be calculated from:

$$\delta(x) = \left(\frac{\eta x}{\rho u}\right)^{\frac{1}{2}} \tag{3.31}$$

where η = gas viscosity
ρ = gas density
u = gas stream velocity parallel to the substrate

The average boundary layer thickness, in the boundary layer model from Prandtl,[49] over the whole plate can then be calculated as follows:

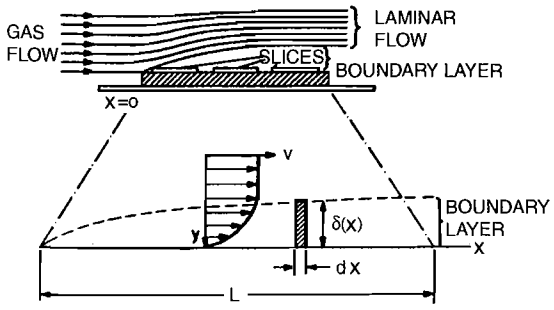

Figure 3.14 Development of a boundary layer in gas flowing over a flat plate. The inset shows an expanded view of the boundary layer. (From R. A. Granger, *Fluid Mechanics*, 1995.[49] Reprinted with permission.)

$$\delta = \frac{1}{L}\int_0^L \delta(x)dx = \frac{2}{3}L\left(\frac{\eta}{\rho u L}\right)^{\frac{1}{2}} \tag{3.32}$$

where L = length of the plate receiving the deposit

The dimensionless Reynolds number, *Re*, is a most important figure in fluid dynamics, characterizing the nature of a fluid flow (gas or liquid). It is given by:

$$Re = \frac{\rho u L}{\eta} \tag{3.33}$$

It equals the ratio of the magnitude of inertial effects to viscous effects in fluid motion (see also Chapter 9). For low values (<2000), the flow regime is called *laminar*, while for larger values, the regime is *turbulent*. Substituting Equation 3.33 in Equation 3.32, we obtain:

$$\delta = \frac{2L}{3\sqrt{Re}} \tag{3.34}$$

By substituting this value for the average boundary layer thickness in Equation 3.5 (i.e., with $dx = \delta$) the following expression for the materials flux to the substrate results:

$$F = -D\frac{\Delta C}{2L}3\sqrt{Re} \tag{3.35}$$

According to Equation 3.35, the film growth rate in the mass flow controlled regime should depend on the square root of the gas velocity, u (since the Reynolds number is proportional to u). Figure 3.15A shows a plot of silicon growth rate as a function of the gas flow rate (proportional to the gas velocity in a fixed volume reaction chamber) and illustrates the predicted square root dependence.[50] At high flow rates, the growth rate reaches a maximum and them becomes independent of flow. In this regime, the reaction rate controls the deposition, evidenced by the exponential dependence of the growth rate on temperature observed at those flow rates (see Figure 3.15B).[50]

Surface reactions can be modeled by a thermally activated phenomenon proceeding at a rate, R, given by:

$$R = R_0 e^{-E_a/kT} \tag{3.36}$$

where R_0 = frequency factor
E_a = activation energy in eV
T = temperature in kelvins

From the slope of an Arrhenius plot, as demonstrated in Figure 3.15B, the activation energy of the rate-determining surface process can be deduced. For a certain rate-limiting reaction, the temperature may rise high enough for the reaction rate to exceed the rate at which reactant species arrive at the surface. In such a case, the reaction rate cannot proceed any faster than the rate at which the reactant gases are supplied to the substrate by mass

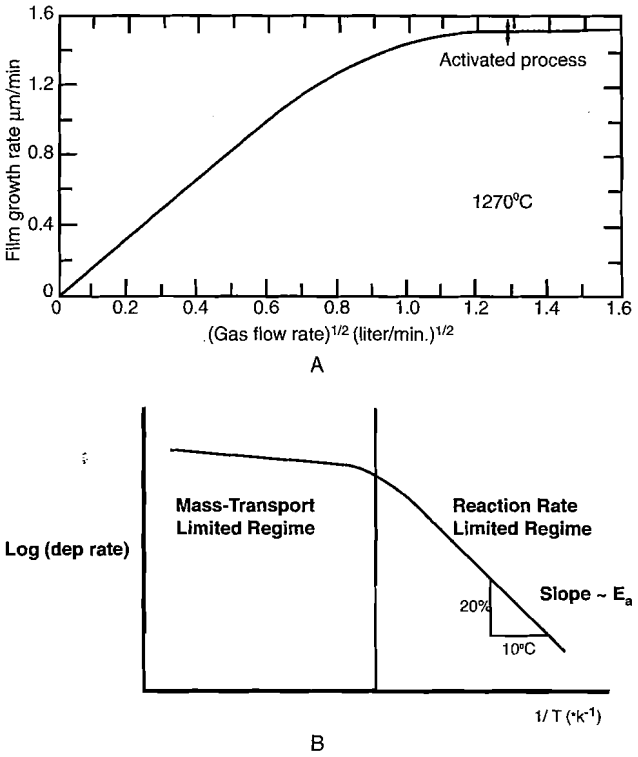

Figure 3.15 Growth rate dependence in a Si CVD process as a function of gas flow rate (A) and temperature (B). (From S. Wolf and R. N. Tauber, *Silicon Processing for the VLSI Era*, 1987.[50] Reprinted with permission.)

transport, no matter how high the temperature is raised (see plateau in Figure 3.15B). This situation is referred to as a *mass-transport-limited deposition process.* Temperature is less important in this regime than it is in the reaction-rate limited (Arrhenius) one. In the latter case, the arrival rate of reactants is less important, since their concentration does not limit the growth rate.

A direct practical application of these two possible rate-limiting processes is the way substrates are stacked in low-pressure CVD (LPCVD) vs. atmospheric pressure CVD (APCVD) reactors. In an LPCVD reactor (~1 Torr), the diffusivity of the gas species is increased by a factor of 1000 over that at atmospheric pressure, resulting in one order of magnitude increase in the transport of reactants to the substrate. The rate-limiting step becomes the surface reaction. LPCVD reactors enable wafers to be stacked vertically at very close spacings as the rate of arrivals of reactants is less important (Inset 3.9). On the other hand, APCVD, operating in the mass-transport-limited regime, must be designed such that all locations on the wafer and all wafers are supplied with an equal flux of reactant species. In this case, the wafers often are placed horizontally (Inset 3.9).

The stability of the flow in a CVD reactor is crucial in achieving uniform deposition. The criterion for flow stability depends on whether the flow is fully developed (i.e., laminar) before it reaches the susceptor. A gas flow is fully developed at a distance l_F from a flat entrance given by

$$l_F = 0.04HRe \tag{3.37}$$

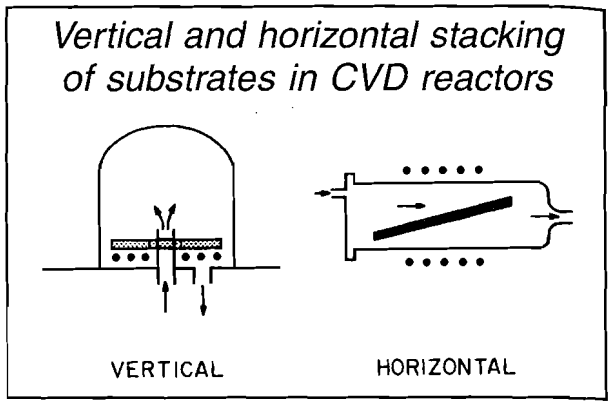

Inset 3.9

where H stands for the height of the flow channel, and Re is based on the channel width. The thermal entrance length l_T for a fully developed radial profile, however, is seven times the velocity entrance length.

$$l_T = 0.28HRe \tag{3.38}$$

The Reynolds number in a typical LPCVD reactor is smaller than that for APCVD. Consequently, the thermal entrance length for APCVD is longer than that for LPCVD reactors.

Step Coverage

The particular flow characteristics around a MEMS feature on a substrate are given by the value of the Knudsen number (Kn), defined in this case as the ratio of the mean free path of the molecules (λ) to the characteristic dimension of the structure to be coated (e.g., the width of the structure). The flow around micromachined features is typically in the transition regime ($0.1 < Kn = \lambda/w < 10$) or in the free molecular regime ($Kn > 10$). For typical CVD growth temperatures, λ may range from ~0.1 μm at atmospheric pressure to >100 μm at 1 Torr. It is anticipated that the thickness of deposited films in the IC industry will reach the order of 10 nm rather than a few microns, and thickness uniformity will be harder and harder to maintain. The tendency is toward large, single wafers that are transferred from station to station in so-called *cluster tools;* considering that no thickness uniformity problem arises when the flow is molecular, it looks like CVD reactors are going to be operated in very low-pressure CVD (VLPCVD) regimes where molecular flow still dominates.

The mean free path of a molecule, λ, based on slightly modified Equation 3.26 (see Problem 3.5), is given by:

$$\lambda = \frac{kT}{2^{\frac{1}{2}} P_T \pi a^2}$$

$$\left(\lambda = \frac{5 \times 10^{-3}}{P_T(\text{torr})} \text{ cm at } 300 \text{ K}\right)$$

$$\left(\lambda = \frac{10^{-2}}{P_T(\text{torr})} \text{ cm at } 600 \text{ K}\right) \tag{3.39}$$

where a is the molecular diameter.[51] The expressions in brackets are easily memorized and come in handy when correlating the total pressure of the system with the mean free path. The above-derived Equation 3.39 is of crucial importance in understanding CVD coating of micromachined features. CVD films have the capacity to passivate or isolate underlying surface features against subsequent layers or the atmosphere, determined by the degree at which edges and pits can be covered uniformly. As demonstrated in the top part of Figure 3.16, three cases can be distinguished. Ideally, a uniform, dense coating should form (Figure 3.16A). This can occur in instances where the reactants, after first hitting the solid, have enough energy left for surface migration before a bond is established with the underlying substrate. Coatings in which equal film thickness exists over all substrate topography, regardless of its slope, provide conformal coverage. In a second case, Figure 3.16B, the mean free path of the molecules is large enough to reach the bottom of the trench, but little energy remains for surface migration. Finally, in the third case, Figure 3.16C, the mean free path length is too short to reach the bottom, and there is little surface migration.

The value of the integral of the material flux in Equation 3.35 ($\int Fld\theta$) and, thus the CVD film thickness, are directly proportional to the range of feasible angles of arrival, θ, of the depositing species (in the absence of surface migration). Different arrival angles in two dimensions are illustrated in the bottom part of Figure 3.16. The arrival angle at a planar surface is 180°. At the top of a vertical step, the arrival rate is non-zero over a range of 270°; the resultant film thickness is 270/180, or 1.5 times greater than that for the planar case. At the bottom corner of a trench, the arrival angle is only 90°, and the film thickness is 90/180 or one-half that of the planar case. The CVD profile in Figure 3.16C, where the mean free path is short compared with the trench dimensions, and there is no surface migration, reflects the 180, 90, and 270° arrival angles. The thick cusp at the top of the step and the thin crevice at the bottom combine to give a re-entrant shape that is particularly difficult to cover with evaporated or sputtered metal. Gas depletion effects also are observed along the trench walls. Along the vertical walls, the arrival angle, θ, is determined by the width of the opening and the distance from the top and can be calculated from:

$$\theta = \arctan\frac{w}{z} \tag{3.40}$$

where w is the width of the opening and z the distance from the top surface (Figure 3.16A). This type of step coverage thins along the vertical walls and may have a crack at the bottom of the step. For uniformity of deposition, in case of Figure 3.16B, where the mean free path is longer than the distance α (the longest path a molecule travels to reach the corner of the trench), the rate of surface migration of adspecies should exceed the rate of adsorption of adspecies. The condition of $\lambda > \alpha$ can be met by working at low pressures (based on Equation 3.39):

$$\frac{kT}{2^{\frac{1}{2}}P_T\pi a^2} > \alpha \tag{3.41}$$

Equation 3.41 gives us the maximum pressure at which $\lambda > \alpha$. The only variable influencing the requirement for large surface migration is the reactor temperature.

Evaporated and sputtered metal films often have trench profiles as shown in the Figure 3.16B, whereas CVD deposited polysilicon and silicon nitride are often uniform and conformal as demonstrated in Figure 3.16A. Plasma deposited SiO_2 and Si_3N_4 are similar to Figure 3.16B.[52]

A simulation model for nonplanar CVD was presented, for example, by Coronell et al.[53] The model provides a picture of the evolution of the depositing film profile. The parameters investigated include the sticking coefficient, the surface mobility of the adsorbed reactants, the Knudsen number (the ratio of the mean free path to the feature size), the feature aspect ratio, and feature geometry.

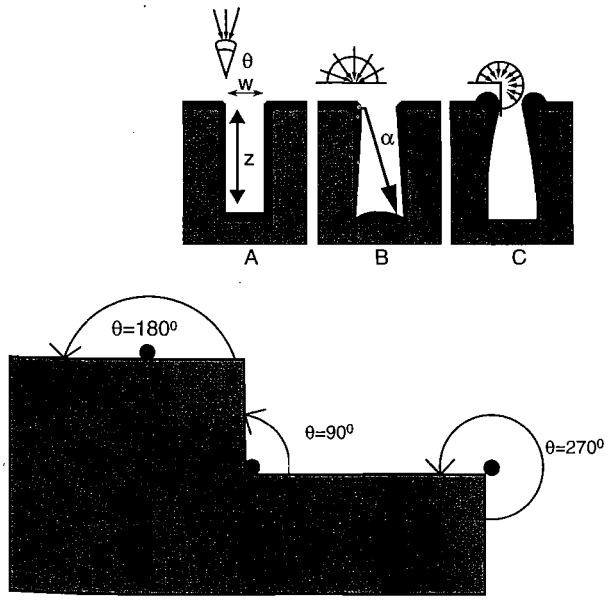

Figure 3.16 Step coverage cases of deposited film. Top: (A) Uniform coverage resulting from rapid surface migration. (B) Nonconformal step coverage for long mean free path and no surface migration. Distance a is the longest path a molecule travels to reach the corner of the trench. (C) Nonconformal step coverage for short mean free path and no surface migration. Bottom: Different arrival angles in two dimensions.

Energy Sources for CVD Processes

Thermal energy is the sole driving force in high-temperature CVD reactors; for lower-temperature deposition, an additional energy source is needed. Radio frequency (RF), photo radiation, or laser radiation can be used to enhance the process, known as plasma-enhanced CVD (PECVD), photon-assisted CVD,[54] or laser-assisted CVD (LCVD),[55] respectively.

With photon- and laser-assisted CVD systems, part of the energy needed for deposition is provided by photons. This method fills the need for an extremely low-temperature deposition process. With a laser source, it is possible to write a pattern on a surface directly by scanning the micron-size light beam over

at 70° for the <111> orientation.[50] These figures represent interesting angles from which to construct micromechanical structures. This selective deposition process also lends itself to CVD, for example, for selective deposition of W.

Epilayer Thickness

Epitaxial layer thickness is a critical parameter both in IC applications and micromachines and therefore must be accurately measured and controlled. Many devices, from discrete transistors and 16-MB DRAMs to membrane-based micromechanical structures, use silicon epitaxial layer wafers as their starting material. The thickness of an epitaxial layer forms an integral part in the design of many micromachined devices. For example, in a piezoresistive pressure sensor, epilayer thickness control ultimately determines the pressure sensitivity control.

Epilayer thickness can be measured from infrared reflectance, angle-lap and stain, tapered groove, weighing, capacitance-voltage measurements, and profilometry. The most widely used nondestructive method of measuring epi thickness is with infrared (IR) instruments. Fourier transform infrared offers automated epilayer thickness measurements.[65]

CVD Equipment

Typical sources for CVD equipment are CVD Equipment Corporation (http://www.cvdequipment.com/) and IonBond Inc. (http://www.ionbond.com/index.html). Commercial epitaxial services offer layers ranging from 0.5 to 150 μm, and N, P, N^+, and P^+ types with a uniformity better than ±5%.

Vacuum equipment to clean, deposit, and etch is being combined more and more in so-called cluster tools (Inset 3.14).[66] Another recent trend in vacuum equipment, along the same line, is the development of continuous in-line stations where raw material goes in at one end and a finished product comes out at the other. The latter goes hand in hand with the concept of a mini-environment (Inset 3.15), loosely defined as an ultraclean space containing only wafers, one or more process chambers, a robot arm for wafer transport, and a few additional accessories. Potential contaminants are thus tightly controlled at the process level itself, while the surrounding area operates under relaxed cleanliness requirements. Mini-environments offer the advantage of keeping humans out of the very clean areas.[67]

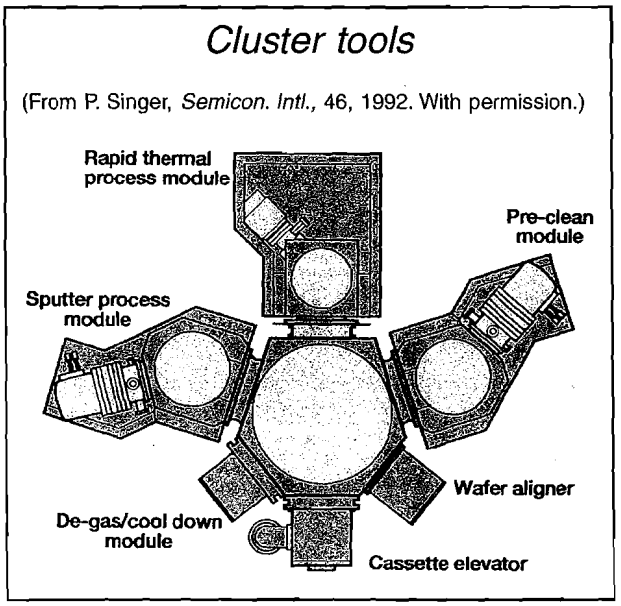

Inset 3.14

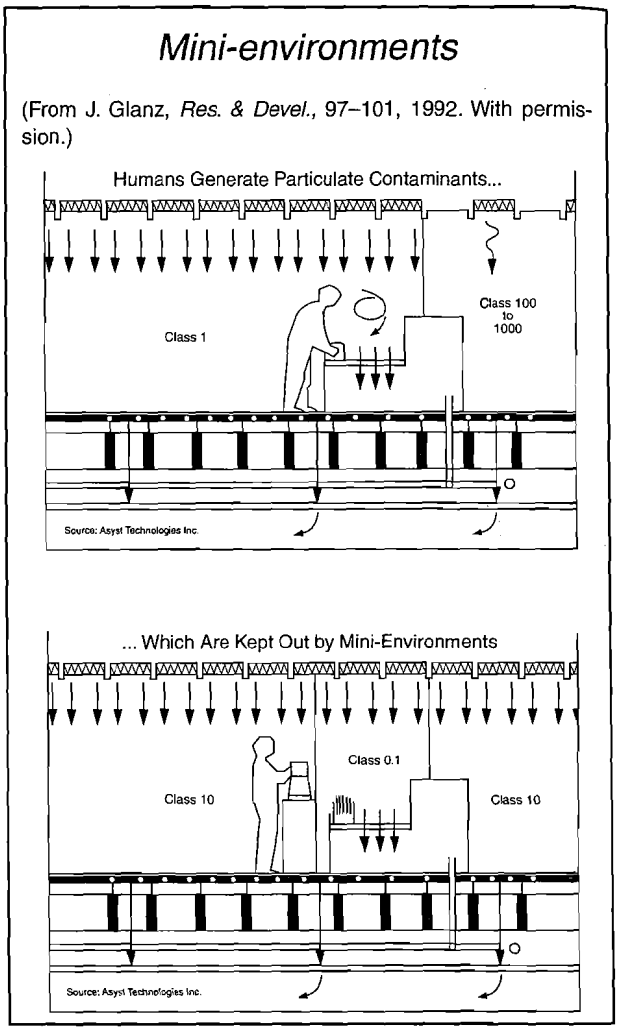

Inset 3.15

Silk-Screening or Screen Printing

Introduction

Screen printing presents a more cost-effective means of depositing a wide variety of films on planar substrates than does integrated circuit technology, especially when fabricating devices at relatively low production volumes. The technique constitutes one of several thick film or hybrid technologies used for selective coating of flat surfaces (e.g., a ceramic substrate). The technology was originally developed for the production of miniature, robust, and (above all) cheap electronic circuits. The up-front investment in a thick film facility is low compared with that of integrated circuit manufacturing. For disposable chemical sensors, recent industrial experience indicates that screen printing thick films is a viable alternative to Si thin film technologies.

How It Works

A paste or ink is pressed onto a substrate through openings in the emulsion on a stainless steel screen (see Figure 3.23A).[68] The paste consists of a mixture of the material of interest, an organic binder, and a solvent. The organic vehicle determines the flow properties (rheology) of the paste. The bonding agent provides adhesion of particles to one another and to the substrate. The active particles make the ink a conductor, a resistor, or an insulator. The lithographic pattern in the screen emulsion is transferred onto a substrate by forcing the paste through the mask openings with a squeegee (Figure 3.23B). In a first step, paste is put down on the screen (Figure 3.24A), then the squeegee lowers and pushes the screen onto the substrate, forcing the paste through openings in the screen during its horizontal motion (Figure 3.24B).[68] During the last step, the screen snaps back, the thick film paste which adheres between the screening frame and the substrate shears, and the printed pattern is formed on the substrate (Figure 3.24C). The resolution of the process depends on the openings in the screen and the nature of the pastes. With a 325-mesh screen (i.e., 325 wires per inch or 40 μm holes) and a typical paste, a lateral resolution of 100 μm can be obtained. For difficult-to-print pastes, a shadow mask may complement the process, such as a thin metal foil with openings. However, the resolution of this method is inferior (>500 μm). After printing, the wet films are allowed to settle for 15 min to flatten the surface while drying. This removes the solvents from the paste. Subsequent firing burns off the organic binder, metallic particles are reduced or oxidized, and glass particles are sintered. Typical temperatures range from 500 to 1000°C. After firing, the thickness of the film ranges from 10 to 50 μm.

A typical silk-screening setup is the one from Universal Instrument Corporation (http://www.uic.com/), the DEK 4265 Horizon Screen. DuPont provides technical tips for screen printing at http://www.dupont.com/mcm/tips/basics.html, and *Screen Printing* magazine can be found at http://www.screenweb.com/resources/toc.html.

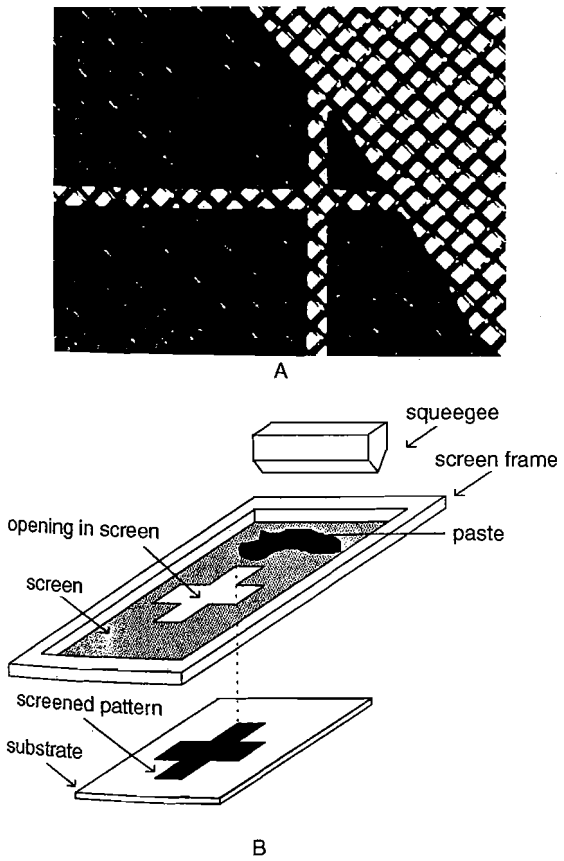

Figure 3.23 Screen-printing. (A) Screen with a 0.002 in line opening oriented at 45° to the mesh weave. (B) Schematic representation of the screen-printing process. (From M. Lambrechts and W. Sansen, *Biosensors: Microelectrochemical Devices*, The Institute of Physics Publishing, 1992.[68] Reprinted with permission.)

Types of Inks

Traditional Inks

Inks are formulated to exhibit pseudoplastic* behavior (Inset 3.16).[69,70] to prevent flowing through the screen until the squeegee applies sufficient pressure. Almost all materials compatible with the high firing temperature, and the other ink constituents can be used to screen print. Different pastes—conductive (e.g., Au, Pt, Ag/Pd, etc.), resistive (e.g., RuO_2, IrO_2), overglaze, and dielectric (e.g., Al_2O_3, ZrO_2)—are commercially available.

The conductive pastes are based on metal particles, such as Ag, Pd, Au, or Pt, or a mixture of these combined with glass. Glass is necessary for the adhesion of the metal conductor to the ceramic (Al_2O_3) substrate. The following conductive pastes can be distinguished by the bonding mechanism utilized.

- Glass-bonded or fritted pastes are inks where adhesion of the metal is achieved with the addition of a glass

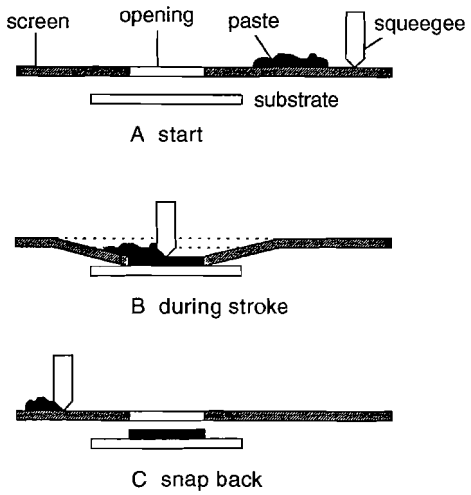

Figure 3.24 The three different steps of the silk-screening process. (From M. Lambrechts and W. Sansen, *Biosensors: Microelectrochemical Devices*, The Institute of Physics Publishing, 1992.[68] Reprinted with permission.)

* In pseudoplastic fluids, viscosity diminishes as the applied velocity gradient increases (see also Chapter 9).

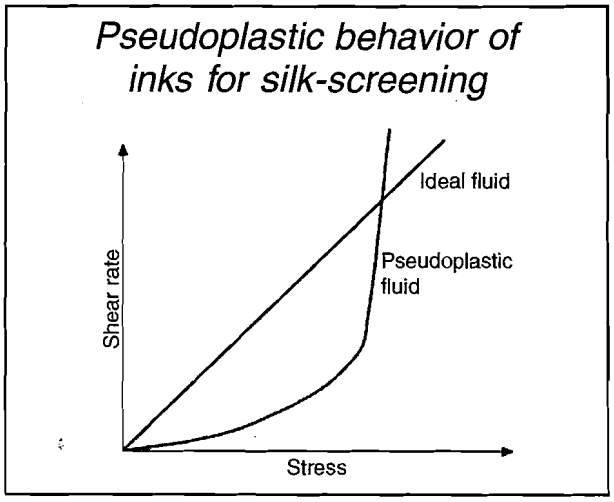

Inset 3.16

mixture (30%) (a typical glass composition is 65% PbO, 25% SiO_2, and 10% Bi_2O_3). A fritted ink contains powdered glass that binds the ink to the substrate material when fired at a temperature of 850°C. Thus, a fritted ink will generally consist of the glass frit, a material defining the desired ink property, and an organic vehicle that renders the ink printable. Vehicles typically consist of solvents mixed with slightly more viscous materials, such as resins, in a ratio designed to give the optimum overall viscosity to the ink.

- Oxides or fritless-bonded inks adhere to the metal via the addition of copper oxide (3%).
- Mixed-bonded pastes are inks for which adhesion is achieved by use of both glass and copper oxide.

Resistive pastes are based on RuO_2 or $Bi_2Ru_2O_7$ mixed with glass (65% PbO, 25% SiO_2, 10% Bi_2O_3). The resistivity is determined by the mixing ratio. Overglaze and dielectric pastes are based on glass mixtures. According to composition, different melting temperatures can be achieved.

Thick film technology with the above type of traditional inks has application in the construction of a wide variety of hybrid sensors, such as sensors for radiant signals, pressure sensors, strain gauges, displacement sensors, humidity sensors, thermocouples, capacitive thick-film temperature sensors, and pH sensors (see Middlehoek et al.[70] and references therein). Also, with Si-based sensors (e.g., pressure sensors and accelerometers) die-mounted on a ceramic substrate, thick film resistors are used for calibration by trimming resistors on the ceramic substrate.

Inks for Chemical Sensors

Inks specifically developed for sensor applications are available or under development. For example, SnO_2 pastes incorporating Pt, Pd, and Sb dopants have been developed for the construction of high-temperature (>300°C) semiconductor gas sensors for reducing gases (so-called Taguchi sensors).[32] Thick metal phthalocyanine films have been deposited on alumina to form the active material in low-temperature (<180°C) gas sensors.[71] For biosensor applications, thick film technology based on pastes that can be deposited at room temperature is crucial. Special grades of polymer-based pastes (e.g., for carbon, Ag, and Ag/AgCl electrodes) are becoming commercially available for this purpose.[72] Polymer thick films with a thickness anywhere from 5 to 50 μm can be screen printed on cheap polymer substrates. The first commercial planar electrochemical glucose sensor (the ExacTech by MediSense, http://www.medisense.de/home.htm) resulted from a screen-printed sensor based on such polymer-based inks (Figure 10.7).

In the research phase of new chemical sensors, pastes must be developed from their pure components. Some examples follow. Pace et al.[73] screen-printed a PVC/ionophore layer for a pH sensor. Belford et al.[74] investigated pH-sensitive glass mixtures and proceeded to screen print them on a multilayer metal conductor to make planar pH sensors. In Pace et al.,[75] a thick film, multilayered oxygen sensor with screen-printed chemical membranes of PVA and silicone rubber is detailed (see also Karagounis et al.[76]). A thick film glucose sensor is presented by Lewandowski et al.[77] and by Lambrechts et al.[68] The latter authors developed an enzyme-based thick film glucose sensor with RuO_2 electrodes. All the above thick film sensors were fabricated on Al_2O_3 substrates. Weetall et al.[78] present an extremely low-cost silk-screened immunosensor on cardboard. Cha et al.[79] compare the performance of thick film Au and Pt electrodes with conventional bulk electrodes.

When faced with adapting a biosensor membrane to an IC process vs. adaptation to a thick film process, it now seems that, once the specialty inks are available, a thick film approach is easier, less expensive, and more accessible. For chemical sensors in which small size is not as important, we expect more research to result in a switch from the overly ambitious IC approach to the more realistic thick film approaches as sketched above. At the end of this chapter, we compare the pros and cons of the two technologies.

Sol-Gel Deposition Technique

In a sol-gel process, as illustrated in Figure 3.25, solid particles, chemical precursors, in a colloidal suspension in a liquid (a sol) form a gelatinous network (a gel). Upon removal of the solvent by heating a wide variety of differently shaped glasses or ceramics result. Both sol and gel formation are low-temperature processes. For sol formation an appropriate chemical precursor is dissolved in a liquid, for example, tetraethylsiloxane (TEOS) in water. The sol is then brought to its gel-point, that is, the point in the phase diagram where the sol abruptly changes from a viscous liquid to a gelatinous, polymerized network. In the gel state the material is shaped (e.g., a fiber or a lens) or applied onto a substrate by spinning, dipping, or spraying. In the TEOS case a silica gel is formed by hydrolysis and condensation using hydrochloric acid as the catalyst. Drying and sintering at temperatures between 200 to 600°C transforms the gel into a glass, and then densification into silicon dioxide.

In MEMS sol-gel methods have been used, for example, in the fabrication of piezoelectrics such as lead-zirconium-titanate (PZT) (see Chapter 9). Also, a commercially available, room temperature chemical gas sensor (a CO fire alarm), is fabricated with the sol-gel process [available from Quantum Group Inc.

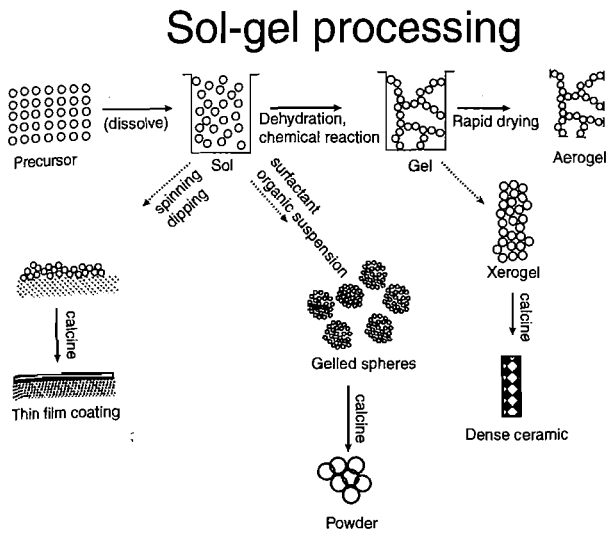

Figure 3.25 Basic flow of a sol-gel process. Surfaces may be coated with optical absorption or index-graded antireflective coatings using this type of methodology.

(http://www.qginc.com/)]. The Sol-Gel Gateway at http://www.solgel.com/bookstore/bookstore.htm is an excellent take-off point for further study of the sol-gel technique on the web.

Doctor's Blade or Tape Casting

Doctor's blade technology, or tape casting, is a continuous chemical fabrication method employing green ceramic tape on a moving substrate, typically another ceramic. A ceramic slurry is continuously dispensed onto the moving substrate from a hopper or other appropriate plumbing. The substrate and dispensed product then move under the doctor's blade, an adjustable gate with a precisely controlled height. The purpose of the doctor's blade is to limit the slurry to a known thickness of material. After drying and removal of the organic content of the green ceramic part by a controlled sinter process, flat and very thin ceramic tapes are obtained. Tape stacks are produced by lamination of several single green tapes under heat and pressure. Tape casting technology may be used for the production of dense and porous ceramic and metallic membranes (alumina, tungsten, molybdenum, silver, and combinations of these materials). Furthermore, ceramic tapes can be processed by cutting, punching, laminating, sintering, etc. A simplified drawing illustrating tape casting is shown in Figure 3.26. The method is surveyed in more detail in Chapter 7.

Plasma Spraying

Introduction

Except for silk-screening, spray pyrolysis, sol gel, and tape casting, all of the above-described additive techniques pertain to thin film fabrication in the IC industry. Microstructures can also be crafted economically with non-IC equipment and materials.

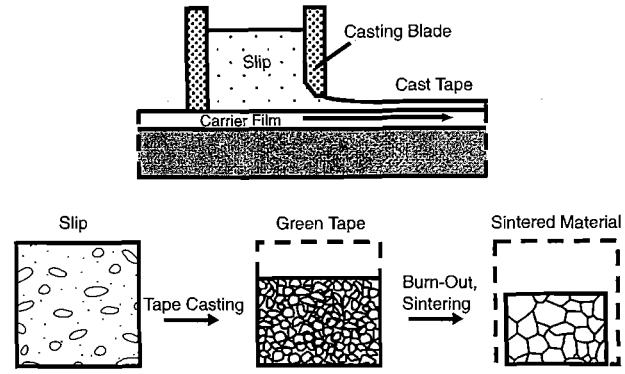

Figure 3.26 Tape casting. The top schematic drawing illustrates tape casting. The bottom sketch shows the different stages during the processing: the slip consisting of water, ceramic particles and binder; the cast, dried green sheet; and finally, the microstructure of the sintered material.

Because of the need to incorporate more and different materials in a thickness ranging anywhere from monolayers to a few hundred microns, micromachinists are broadening their horizon beyond IC deposition techniques and increasingly are incorporating hybrid methodology in their tool boxes. Spray pyrolysis (see above), drop delivery systems (see below), and pick-and-place technology are but a few examples. Here we review plasma spraying as another example of a non-IC tool for chemical sensor fabrication. With plasma spraying, almost any material can be coated on many types of substrate. Applications include corrosion- and temperature-protective coatings, superconductive materials, and abrasion resistance coatings.[16] Today, turbine blades and other components of aircraft engines are plasma coated with corrosion- and temperature-resistant coatings.

How It Works

All the CVD and PVD techniques discussed so far, except for the cluster deposition method discussed above, rely on atomistic deposition; that is, atoms or molecules are individually deposited onto a surface to form a coating. Plasma spraying is a typical particle deposition method; particles, a few microns to 100 μm in diameter, are transported from source to substrate. The basic configuration of a plasma-arc torch setup for layer deposition and a plasma spray nozzle setup are shown in Figures 3.27 and 3.28, respectively.

In plasma spraying (Inset 3.17), a high-intensity plasma arc is operated between a stick-type cathode and a nozzle-shaped, water-cooled anode as illustrated in Figure 3.28. For atmospheric spraying, one typically works at power levels from 10 to 100 kW. Plasma gas, pneumatically fed along the cathode, is heated by the arc to plasma temperatures, leaving the anode nozzle as a plasma jet or plasma flame. Argon and mixtures of argon with other noble (He) or molecular gases (H_2, N_2, O_2, etc.) are frequently used for plasma spraying. Fine powder suspended in a carrier gas is injected into the plasma jet where the particles are accelerated and heated. The plasma jet may reach temperatures of 20,000 K and velocities up to 1000 ms^{-1}. The

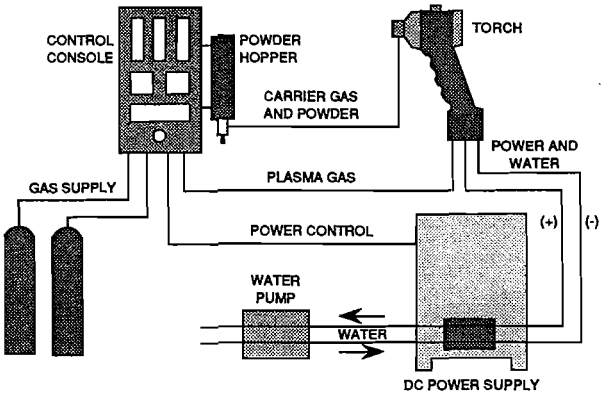

Figure 3.27 Setup for plasma spray.

temperature of the particle surface is lower than the plasma temperature, and the dwelling time in the plasma gas is very short. The lower surface temperature and short duration prevent the spray particles from being vaporized in the gas plasma. The particles in the plasma assume a negative charge, owing to the different thermal velocities of electrons and ions. As the molten particles splatter with high velocities onto a substrate, they spread, freeze, and form a more or less dense coating, typically forming a good bond with the substrate. The resulting coating is a layered structure (lamellae). As shown in Figure 3.28A, the particle goes through different regions of temperature and flow velocity. Ideally, the particles should arrive at the substrate at high velocities in a completely molten state to form the densest coating with little porosity. To produce porous films for the fabrication of oxygen sensors in our own work,[80] we

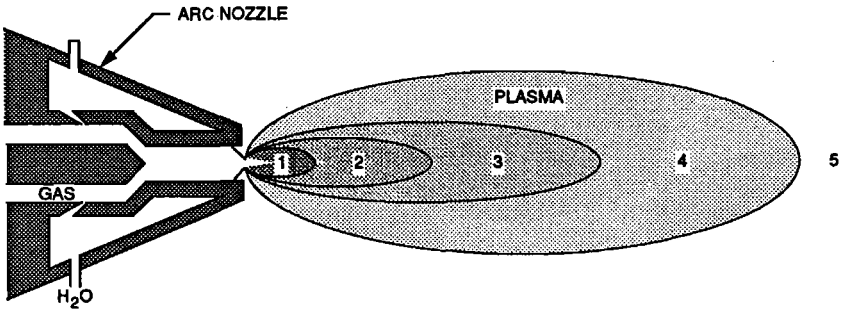

REGION	DISTANCE FROM NOZZLE	TEMPERATURE RANGE (K)	LINEAR FLOW VELOCITY (m/s)
1	< 1 cm	1.5×10^4 — 1×10^4	~ 400
2	1 < d < 5 cm	1×10^4 — 5×10^3	~ 400 — 200
3	5 < d < 10 cm	5×10^3 — 2×10^3	~ 200 — 100
4	10 < d < 20	2×10^3 — 1×10^3	< 100
5	20 < d	< 500	

A

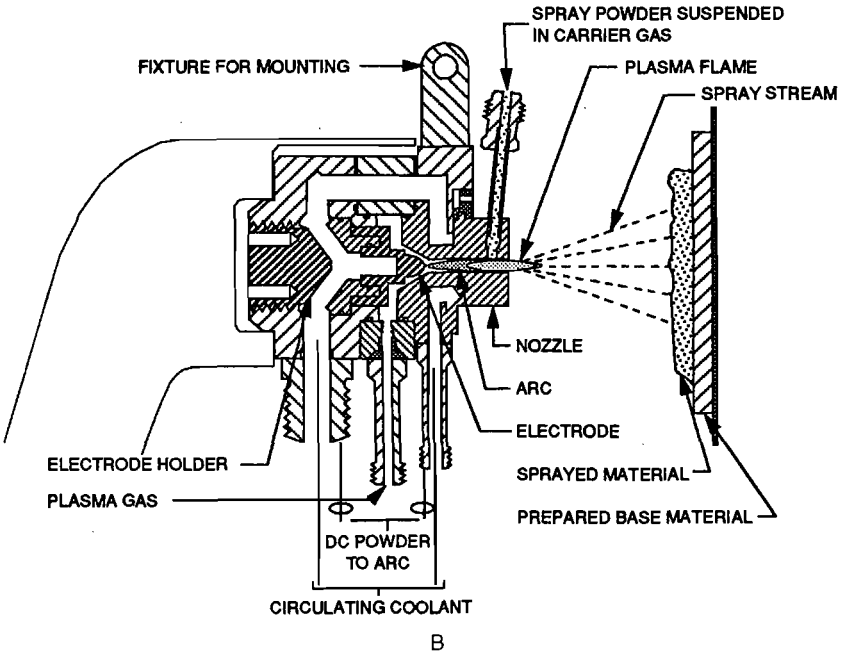

B

Figure 3.28 Plasma spray nozzle. (A) Typical ranges of temperature and flow velocity with distance from the nozzle. (B) Torch for powder spraying.

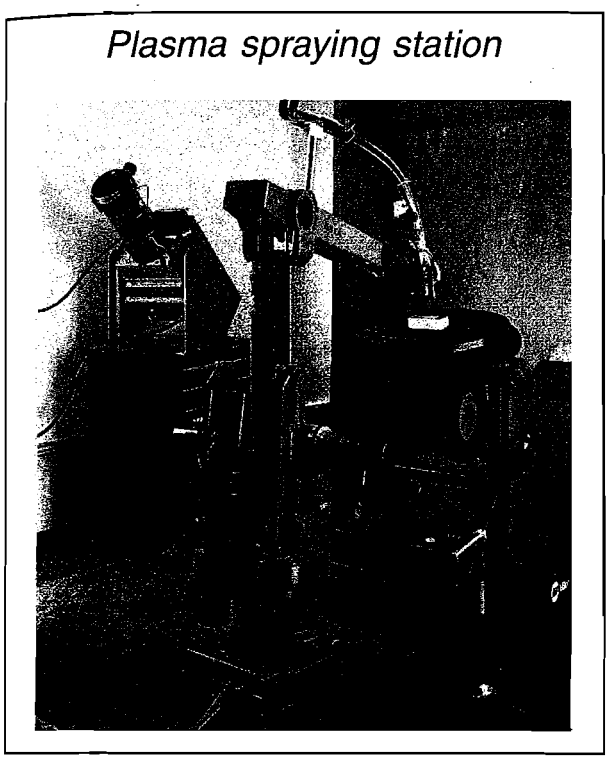

Inset 3.17

positioned the substrate somewhere between regions 4 and 5. To produce dense films, we positioned the substrate in region 4. With this technique, a minimum thickness is about 25 μm and very thick coats up to a few millimeters thick are possible. When attempting to deposit gas-sensitive layers such as ZrO_2 on thermally isolated, thin Si membranes to make a power efficient gas sensor, we found that the kinetic energy of the plasma was too high, and it broke the thin, suspended Si membranes. The high temperature and kinetic energy preclude the potential for integrating Si with high-temperature plasma spraying. Later, in Example 3.2, we will demonstrate how plasma spraying of yttria stabilized zirconia may be used in the batch fabrication of all solid state oxygen sensors.

Plasma spraying equipment maybe purchased, e.g., from SULZER METCO (http://www.sulzermetco.com/index.html).

Deposition and Arraying Methods of Organic Layers in BIOMEMS

Introduction

Today, miniaturization methods are more and more often applied to biotechnology problems. With the growth of the "BIOMEMS" field, techniques for depositing organic materials for chemical and biological sensors, often arranged in some type of an array configuration, are gaining importance, and materials rarely dealt with in the IC industry are encountered. Organic gas permeable membranes, ion selective membranes, hydrogels, and organic monolayers are needed for the manufacture of room-temperature gas sensors, ion selective electrodes (ISEs), enzyme sensors, immunosensors, and DNA and protein arrays. Their deposition presents challenges not typically encountered in the IC world. Membranes may be based on classical polymers, such as PVC (polyvinylchloride), PVA (polyvinylalcohol), PHEMA (polyhydroxyethylmethacrylate), or silicone rubber, and incorporate pH and temperature-sensitive biological materials such as enzymes, antigens, and antibodies. Single layers of molecules may be deposited by Langmuir–Blodgett (LB) deposition techniques or as self-assembled monolayers (SAMs). Those LB films or SAMs may then be further used as anchor points for proteins or DNA probes, and the latter polymer molecules may be synthesized *in-situ*. Because of the importance of this emerging field, we briefly review the different options available to coat and pattern organic materials on various substrates. For the organic film deposition techniques reviewed earlier in this Chapter, we provide a short summary only.

Deposition Methods for Organic Materials

Spin Coating

Spin coating technology has been optimized for deposition of thin layers of photoresist, about 1 to 2 μm thick, on round and nearly ideally flat Si wafers. Resists are applied by dropping the resist solution, a polymer, a sensitizer (for two-component resists), and a solvent on the wafer. The wafer is then rotated on a spinning wheel at high speed so that centrifugal forces push the excess solution over the edge of the wafer, and a residue on the wafer remains due to surface tension. In this way, films down to 0.1 μm can be made. An empirical expression relating film thickness to solution viscosity and rotation speed was given in Chapter 1, on lithography (Equation 1.1). However, biosensor substrates rarely are round or flat, and many chemical sensor membranes require a thickness considerably greater than 1 μm for proper functioning. For example, a typical ion selective electrode (ISE) membrane is 50 μm thick. Consequently, spin coating technology does not necessarily fit in with thick chemical membranes on a variety of substrates, and for monolayer deposition the method is not adequate, either. For a tutorial on spin coating, visit http://www.mse.arizona.edu/faculty/birnie/Coatings/index.htm.

Dip Coating

Dip coating of a substrate in a dissolved polymer typifies the simplest method to apply an organic layer to a substrate. It is especially suited for wire-type ion selective electrodes (ISEs) and enzyme-based biosensors where the membrane forms a droplet at the end of a wire. A substrate (for example, a chloridized silver wire) is dipped into a solution containing the polymer and a solvent. After evaporation of the solvent, a thin membrane forms on the surface of the sensor. To obtain pinhole-free membranes, the dipping is repeated several times, interspersed with drying periods. Even though the eventual goal is typically the production of a planar sensor structure, an Ag wire may be applied in the research phase to quickly evaluate a new membrane composition. The method is difficult to commercialize due to the variability in coating thickness and uniformity. As shown in Figure 3.25, dipping and spinning is also used in the

sol–gel process. For further reading on dip coating, visit http://www.solgel.com/articles/Nov00/mennig.htm.

Plastic Spraying

Plastic spray-coating techniques may involve liquids, gases, or solids. Spray coating of a liquid involves pressurization by compressed air or, in an airless method, pushing liquid mechanically through tiny orifices. Vapors are carried in an inert dry vapor carrier. In the case of a solid, a powdered plastic resin is melted and blown through a flame-shrouded nozzle. Such thermal spray coating involves heating a material, in powder or wire form, to a molten or semi-molten state. The material is propelled using a stream of gas or compressed air to deposit it on a substrate. The coating material may consist of a single element but is often a composite with unique physical properties that are only achievable through the thermal spray process. There are two main classes of powder coatings: thermosetting and thermoplastic coatings. In a thermosetting film, cross-linking occurs between the molecules in the powder during baking. This cross-linking turns the baked film into a single giant molecule that can't melt or flow. In a thermoplastic film, thermal energy makes the binder molecules mobile enough to become entangled so that a continuous film forms and this film hardens upon cooling. While a thermoplastic film can still melt or flow, it can do that only at elevated temperatures. The powders are often given electric charges during spraying so that electrostatic forces will hold them in place until they're baked on. In electrostatic spraying, a negatively charged plastic powder is spray gunned onto grounded conductive parts.[11]

Thermoplastic and thermosetting coatings may also be formed by dipping a heated part into a container of resin particles set in motion by a stream of low-pressure air (fluidized-solid bed). This method is only of use if an inert coating is desired, for example, for biocompatibility but not for heat sensitive functionalized coatings.

Thermal spraying is ideally suited for large structures that otherwise could not be dipped in a polymer suspension (see above). Unlike electrostatic powder coatings, nonconductive components can be coated and, unlike fluidized bed coatings, heat sensitive materials (aircraft skins) can be sprayed. Polymer coatings can be repaired by heating (for remelting or curing) and by applying additional material to the desired location. Polymer coatings can be applied in high humidity as well as at temperatures below freezing. Certain polymers have excellent adhesion to metallic surfaces due to interfacial bonding. Metals, ceramics, or other polymers can be incorporated into the polymer matrix during spraying to act as a filler.

Casting

Casting is based on the application of a given amount of dissolved material on the surface of a sensor substrate and letting the solvent evaporate. A rim structure is fashioned around the substrate, providing a "flat beaker" for the solution. This method provides a more uniform and a more reproducible membrane than dip coating. Membranes in planar ion selective electrodes (ISEs) are often made this way. Casting is also often employed to obtain thicker photoresist layers than typically is possible with spin coating (see also Chapter 6).

Doctor's Blade or Tape Casting

Doctor's blade technology or tape casting is a continuous fabrication method that can be used not only for ceramics, as shown in Figure 3.26, but may also be applied to organics such as hydrogels and all types of organic cocktails, for example to make enzyme based biosensors. As an application of a doctor's blade process in BIOMEMS, consider the mass production of amperometric glucose sensors. Using a silicon batch approach, it is almost impossible to make a glucose sensor for less than $1 (or any disposable biosensor for that matter!). The current industrial process to make glucose sensor strips involves doctor's blade on a continuous moving web, making a $.10 cost per sensor possible.

One of the many challenges in BIOMEMS is the fabrication of affordable disposable biosensors, and this may be accomplished by incorporating continuous processes such as tape casting in future micromachining methods. An example of such a process for biosensor manufacture on large plastic sheets, and eventually on a moving web, is shown in Figure 3.44 (Example 3.3). The process illustrated allows for the fabrication of a sensor array composed of sensors that may otherwise have fabrication incompatibilities. We call this futuristic BIOMEMS approach "beyond batch."

Glow Discharge (Plasma) Polymerization

During glow discharge, polymerization of polymer films ensues from plasmas containing organic vapors. Figure 3.29 illustrates the setup we used in our own work on plasma polymerization of doped polymers. The apparatus consisted of a quartz tube reaction chamber; a gas-handling system to introduce the carrier gas, monomer, and dopant into the system as well as to remove the unreacted material; and a power supply (operating at 27 MHz) to provide the RF energy necessary to create and maintain a plasma within the system. Despite the complex chemistry of this process, good conformal coatings often result.

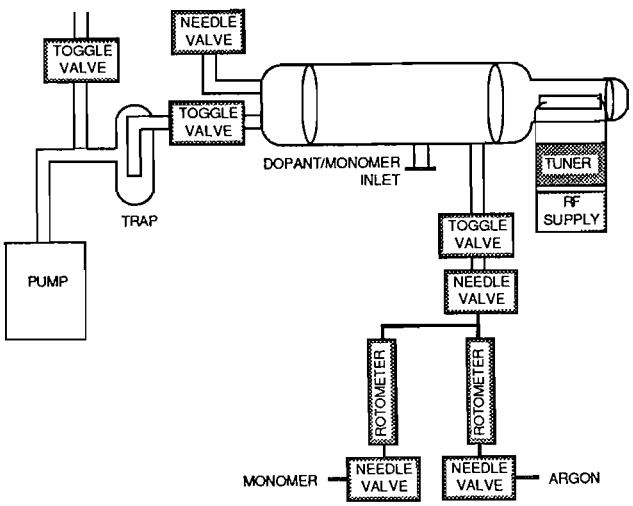

Figure 3.29 Schematic of plasma deposition system.

Guckel applied this technique to obtain deposition of PMMA in layers >100 μm.[81] In research at SRI International, we synthesized electro-active plasma polymers using I_2 or N_2O as dopants from the following monomers: thiophene, furan, aniline, benzoaldehyde, benzene, indole, diphenylacetylene, and 1-methylpyrrole.

In general, plasma-polymerized materials offer the following advantages:

- The plasma-polymerized films are uniform, pinhole-free, chemically resistant, and mechanically strong.
- A thin to thick film (200 Å to >100 μm) can be formed in a flawless manner at ambient temperature onto any substrate.
- The organic film deposited by the plasma process adheres strongly to the substrate.
- The choice of monomers is unlimited; almost any organic compound convertible into vapor can be polymerized.
- The plasma process (one-step process from a vapor source) is compatible with conventional CMOS technology.
- Some functional groups can be introduced onto the surface of the organic film by subsequent glow discharge treatment in a reactive gas atmosphere.
- Highly irregular surfaces can be coated and patterned by depositing a light-sensitive polymer by plasma polymerization (e.g., polymerized PMMA).

For more details on plasma polymerization, see, for example, Yasuda in reference.[15]

Langmuir–Blodgett and SAM Approach

The use of monolayer electron-beam resists, as discussed in Chapter 1, affords nanometer-scale lithography resolution. The chemical sensor industry exploits monolayers of organics for use, for example, in immunosensors and to provide anchor points for subsequent organic molecules or membranes. The technique, invented by Irving Langmuir and Katharine Blodgett in 1935, allows the controlled deposition of monomolecular layers. This ultrathin film deposition technique is limited to materials that consist of amphilic long chain molecules with a hydrophobic molecule at one end and a hydrophilic molecule at the other.

In the Langmuir–Blodgett process, a monolayer of film-forming molecules (stearic acid is a model molecule) on an aqueous surface is compressed into a compact floating film and transferred to a solid substrate by passing a substrate through the water surface at a constant speed and film surface tension (Figure 3.30). Thus, layered films can be built up in thickness (up to 100 layers) by consecutive dippings in the Langmuir trough. Phthalocyanine films sensitive to oxidizing gases such as NO_2 and biological materials sensitive to odors resulted via this method. Most of the difficulties with Langmuir–Blodgett films stem from the need to make the material pinhole-free and to overcome the problem of their lack of mechanical, chemical and thermal stability.

Self-assembled monolayers (SAMs) of alkanethiols and disulfides on gold, as we saw in Chapter 1, form organic interfaces with properties largely controlled by the end groups of the molecules composing the film. This method of building monolayers forms an important alternative to the Langmuir–Blodgett method. SAMs on gold are generally more stable and can better withstand strong acids and bases, they are not destroyed by solvents and can withstand physiological environments.[82]

Patterning of Organic Materials

Introduction

In the previous sections, we summarized the different methods available to deposit organic thin layers. In what follows, we will encounter some of the same techniques and introduce some new ones as we look into the process of depositing small amounts of material in a well defined, small spot on a substrate; i.e., the patterning of organic films. Patterning of organic thin layers into discrete array elements has recently spawned a wide variety of applications. These range from sensor arrays for electronic noses and tongues to DNA and protein arrays.

Patterning through Photolithography

Patterning of Hydrogels, Gas Permeable Membranes, and Ion Selective Electrodes

Spinning, UV exposure, and development of resists are well known, low-cost, mass-production patterning procedures in photolithography for IC fabrication. Naturally, this approach became one of the first methods to be applied to the patterning of other organic materials. However, photosensitized organic materials such as hydrogels, gas permeable membranes, and ion selective electrodes, e.g., to fabricate a biosensor array, are usually not commercially available. To cope with this problem, photosensitive materials from high-purity materials must be prepared. For example, to pattern a hydrogel, e.g., as a water-soluble polymer like polyvinyl alcohol (PVA), a photosensitizer such as $(NH_4)_2Cr_2O_7$ must be added.[68] After spin coating, the polymer film is photochemically cross-linked by UV light. In the exposed regions, an insoluble hydrogel materializes. The development or removal of unexposed regions is carried out in warm water. A recent example of patterning a hydrogel actuator material inside a fluidic network through the use of photolithography is described by Liu et al.[83] The actuator hydrogel, after in-situ photopolymerization, responds to changes in local pH by changing its volume and thus provides a means for valving action in the fluidic network.[84] The in-situ polymerization of these polymeric valves and their function in a fluidic network are demonstrated in Figure 3.31.

An alternative approach to patterning organic materials without modifying the material through the addition of a photosensitizer is through lift-off. Lift-off to lithographically pattern hard to etch materials (e.g., Pt), or in general to pattern materials that are not photosensitive, was introduced in Chapter 1. At one time, a problem with lift-off for patterning organic materials was the thickness required for the patterning

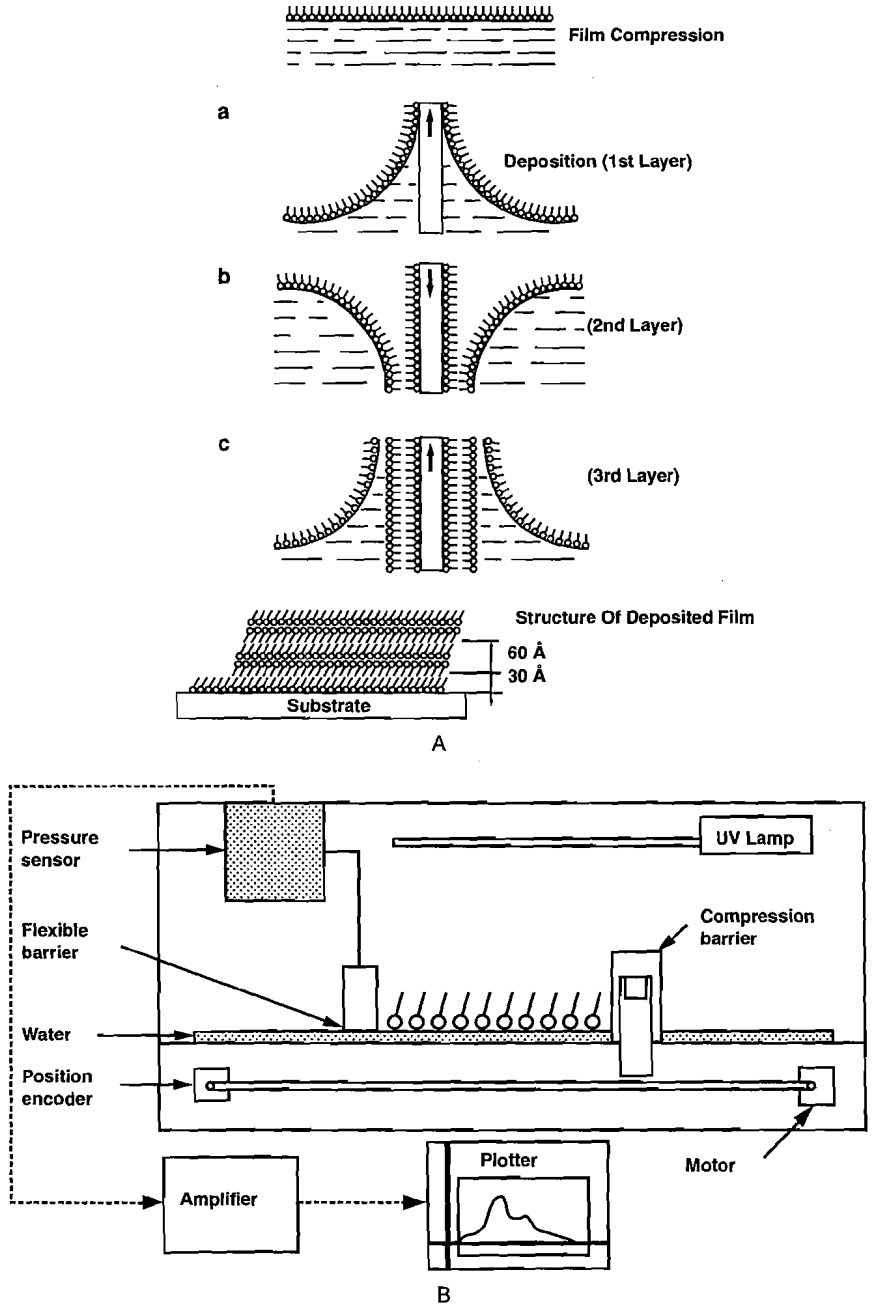

Figure 3.30 Langmuir–Blodgett film deposition: (A) sequence of a deposition; (B) apparatus.

photoresist layer. As discussed earlier, a typical resist layer once measured only about 1 μm thick, whereas the thickness needed for the organic layers involved in chemical sensors frequently can reach up to 100 μm, demanding resist layers that are thicker yet. The many new thick resist technologies now available could make this approach more feasible today. A remaining problem with lift-off, though, is that it can be used only with materials that are resistant to the solvent necessary for the resist removal, so this technology probably will be limited to specific cases.

Hydrogels, gas permeable membranes, and ion selective electrodes are all relatively thick—from several microns to a 100 μm. Next, we consider patterning of much thinner organic l ers such as monolayers of DNA and proteins.

Very Large Scale Immobilized Polymer Patterning and Synthesis

Affymax's *very large scale immobilized polymer synthe* (VLSIPS) is illustrated in Figure 3.32. The technique patter and synthesizes biopolymers at the same time.[85] In the case a light-directed oligonucleotide synthesis for a DNA array (t GeneChip), a solid support (e.g., a 1.28 × 1.28 cm Si chip) derivatized with a covalently linked aminosilanated layer t minated with a photolabile protecting group. The on-ch

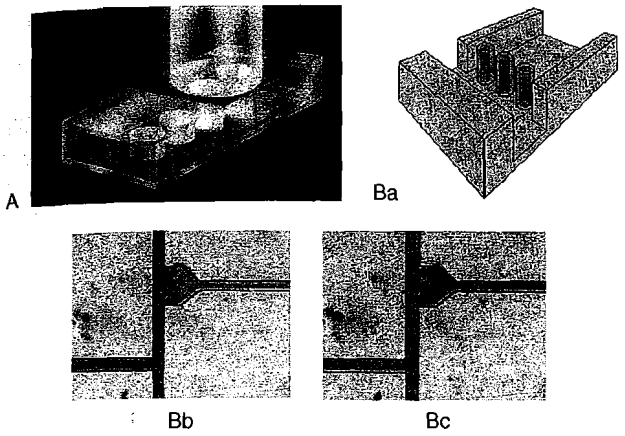

Figure 3.31 Patterning Hydrogels. (A) A schematic showing the in-channel photo-polymerization technique. (Ba) Schematic of a 2D shut-off microvalve consisting of hydrogel "jackets" (50 μm thick) around three prefabricated SU-8 posts. (Bb) Micrograph of the hydrogel jackets blocking the regulated channel (pH 7) in their expanded state in a pH 12 solution (dyed). (Bc) Micrograph showing the contracted hydrogels allowing fluid to flow down the side branch. (This figure also appears in the color plate section following page 394.) (Courtesy of Dr. D. Beebe, University of Madison, Wisconsin.)

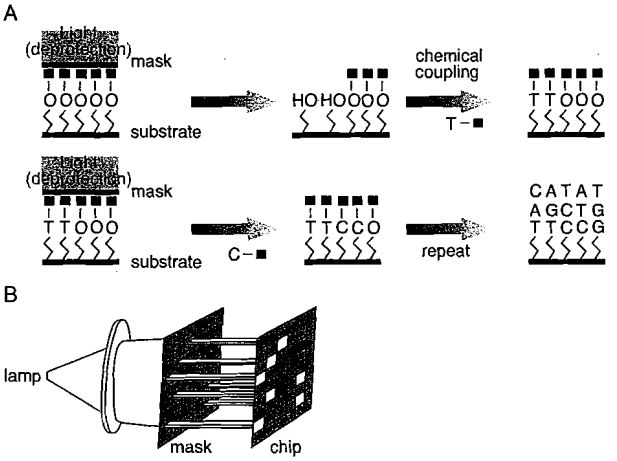

Figure 3.32 Very large scale immobilized polymer synthesis (VLSIPS). Micro- and nanopatterned protein surfaces. (A) Photo-deprotection patterning scheme. Light directed oligonucleotide synthesis. A solid support is derivatized with a covalent linker molecule terminated with a photolabile protecting group. Light is directed through a mask to deprotect and activate selected sites, and protected nucleotides couple to the activated sites. The process is repeated, activating different set of sites and coupling different based allowing arbitrary DNA probes to be constructed at each site. (*B*) Schematic representation of the lamp, mask and array. (After P. A. S. Fodor et al., *Science*, 251, 767–773, 1991.[85])

combinatorial synthesis proceeds by photolithographically deprotecting all array elements that are to receive a common nucleoside, coupling that nucleoside by exposing the entire array to the appropriate phosphoramidite, and then, after the oxidation and washing steps, repeating the procedure for the next nucleoside. To make an array of N-mers requires 4N cycles of deprotection and coupling, one for each of the four bases, times N base positions. This photolithographic method requires 4N masks, which are specific to the pattern of sequences on the array but can be used to make many copies of the array. The masks add considerable expense, and the procedure is best suited for generating large numbers of identical arrays. By going through 32 iterations of the oligonucleotide synthesis, 65,536 oligos containing 8 units can be fabricated in about a day.

The previously described combinatorial approach to fabricating DNA arrays can also be used for peptide synthesis to create an assortment of peptides of almost any length. The approach is indeed a generic and powerful method to create large numbers of compounds in a very small area.

Protein Patterning with Lithography

A wide range of proteins has been patterned with features in the micrometer meter range by making a surface locally hydrophobic or hydrophilic through lithography (see Chapter 1, under *Very Thin Resist Layers*). Such patterns may be observed by a number of techniques, including fluorescence microscopy, atomic force microscopy, and the growth response of cultured biological cells.[86] There are also efforts to produce nanopatterned protein arrays by using proteins that self-assemble into molecular lattices, such as the bacterial S protein. Douglas et al.[87] used metal-decorated crystals of the S proteins of *Sulfolobus acidocaldarius* as a protein mask to pattern hexagonal arrays of 10-nm dia. holes onto graphite surfaces. Figure 3.33 demonstrates how the self-assembled protein lattice may be used for nanopatterned protein surfaces.

UV lithography, in some special cases, may also work directly for patterning thin protein layers as demonstrated in Example

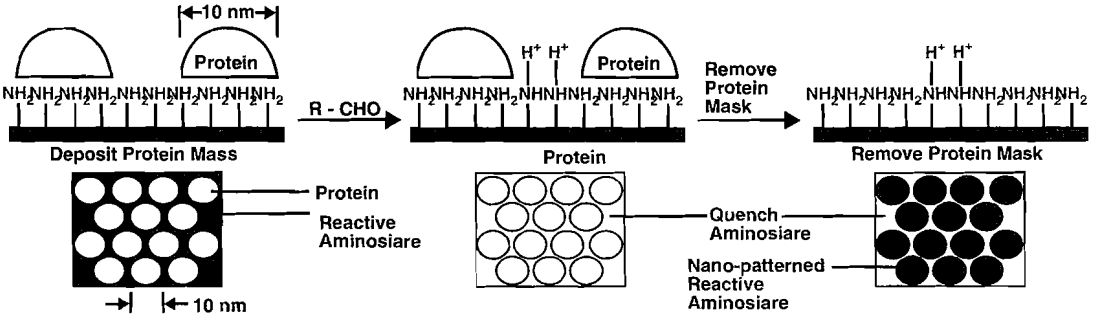

Figure 3.33 Nanopatterning of surface chemistry using a self-assembled protein mask. (After K. Douglas et al., *Science*, 257, 642–644, 1992.[87])

1.1. In this example, a protein grating was created by shining UV, in the presence of oxygen, through a grating photomask. Besides UV lithography, soft and hard x-rays, e-beam, and ion projection lithography can all be used for direct protein film structuring.

Digital Mirror Array Patterning

With VLSIPS, a DNA chip of 25 mers may require as many as 100 different masks, leading to a very high cost and an excessively long fabrication time. Sangeet Singh-Gasson et al. came up with an elegant maskless fabrication alternative for light-directed oligonucleotide micro arrays by using a digital micromirror array.[88] Specifically, this group used the Digital Micromirror Device (DMD) from Texas Instruments (http://www.dlp.com/dlp/default.asp), the fabrication of which is described in Chapter 5. This specific DMD consists of a 600 × 800 array of 16-μm wide micromirrors (the same type is used in computer display projection systems). The tiny mirrors are individually addressable and can be used to create any given pattern or image in a broad range of wavelengths. With a 1:1 imaging system, the DMD can be exploited to address 480,000 pixels on a 10 × 14-mm area. The maskless array synthesizer (MAS) or virtual mask array synthesizer is shown in Figure 3.34. An added benefit of this clever approach is that the active surface of the glass substrate can be mounted in a flow cell reaction chamber connected to a DNA synthesizer. Chemical coupling cycles follow light exposure, and these steps are repeated with different virtual masks to grow desired oligonucleotides in any desired pattern. It is obvious that the MAS could also be used for other array patterning/synthesis experiments.

Virtual masks are also used by Bertsch et al.[89] at the Swiss Federal Institute of Technology (EPLF). This research group uses a computer-controlled liquid crystal display (LCD) as a dynamic pattern generator in microsterolithography (see some results in the 3D section of Chapter 1). The same approach could be put to use to generate molecular arrays.

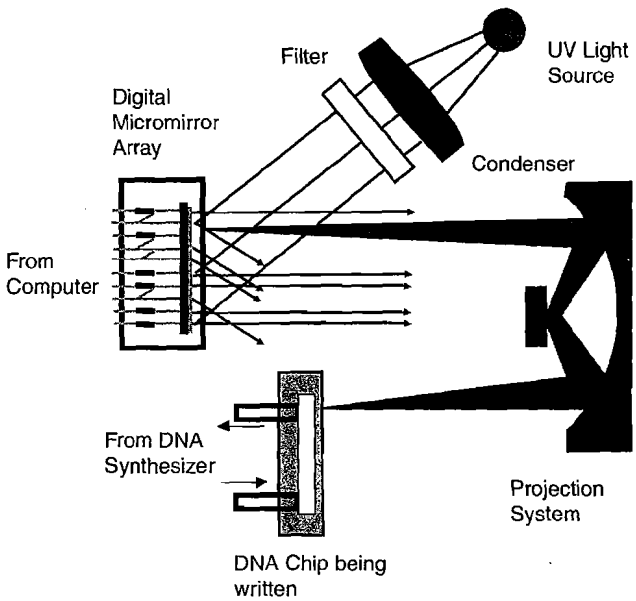

Figure 3.34 Schematic of the maskless array synthesizer (MAS). A UV light source is used to illuminate the digital micromirror array. A reflective Offner relay 1:1 imaging system with a numerical aperture (NA) of 0.08 forms an image of the pattern on the digital micromirror array on the active surface of the glass substrate. The glass substrate is enclosed in a flow cell connected to a DNA synthesizer. (Courtesy of Dr. R. Green, NimbleGen Systems.)

Ink-Jetting and Microspotting

Introduction

Drop delivery systems present an alternative mechanical approach to pattern organic materials on a planar substrate. Although the resolution is lower than with lithography methods, these mechanical methods are faster and less expensive.

Ink-Jet Printing

Drop delivery in BIOMEMS is based on the same principles as commercial ink-jet printing. The ink-jet nozzle is connected to a reservoir filled with the chemical solution and placed above a computer-controlled x-y stage. Depending on the ink expulsion method, even temperature-sensitive enzyme formulations can be delivered. The substrate to be coated is placed on the x-y stage and, under computer control, liquid drops (e.g., 50 μm in diameter) are expelled through the nozzle onto a well defined place on the wafer (see Figure 3.35). Different nozzles may print different spots in parallel. Although these drop delivery systems are serial, they can be very fast, as evidenced by epoxy delivery stations in an IC manufacturing line.

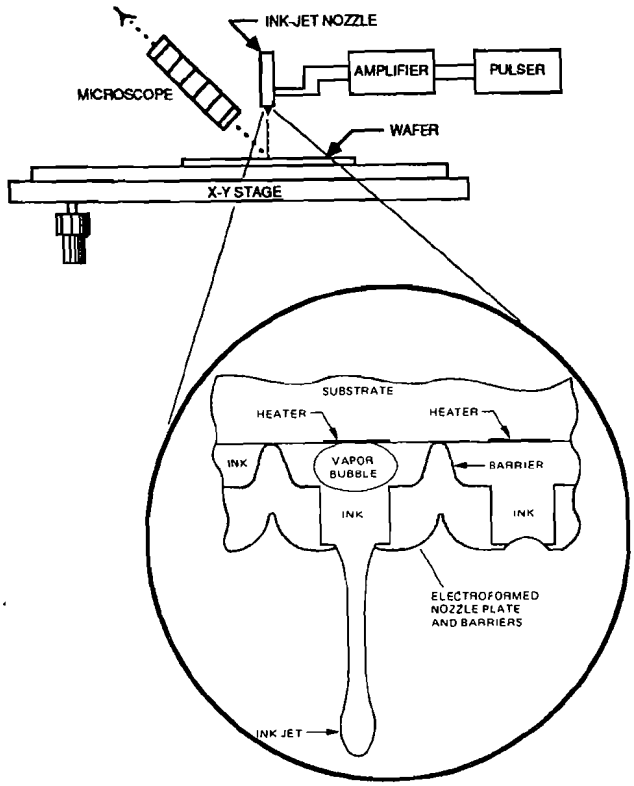

Figure 3.35 Ink-jet deposition system.

The ink-jet mechanism in Figure 3.35 is thermal and is often called a *bubble jet,* with droplets as small as a few picoliters (24 pL).[90] HP's thermal ink jet (TIJ) represents the state of the art in this arena. In the TIJ, tiny resistors are used to rapidly heat (1,000,000°C/s) a thin (0.1 μm) layer of liquid ink to about 340°C. A superheated vapor explosion vaporizes a tiny fraction of the ink to form an expanding bubble that ejects a drop of ink (and any trapped air) from the ink cartridge onto the paper or other substrate. It is noteworthy that the ink does not actually boil. The bubble collapse and break-off draw fresh ink over the resistor. The bubble formation, expansion, break-off, and refill (all very fast) are illustrated in Figure 3.36A. The HP TIJ has all the active power electronics and orifice addressing integrated on the same Si chip with the drop generator as shown in Figure 3.36B. The orifices are spaced at 300 per inch in a single column, and, for a 600 dpi printhead, two offset columns are employed. It is even possible to put 600 TIJ orifices/inch in a single column. Current piezo ink jets (see next) have only 90 orifices/inch. The TIJ technology is a remarkable piece of engineering. To put this in perspective, engineers trying to develop a commercial ion sensitive field effect transistor (ISFET) have struggled for more than 25 years to integrate liquids with electronics with little success or market acceptance until very recently (see Chapter 10). Not only did HP succeed in integrating liquid with electronics, they were also able to find an effective method of repeatedly heating the liquid (ink). HP has also carved out a very lucrative business in disposable ink cartridges. Perhaps their efforts will also pay of in other fluidic areas, and it may even be worth reconsidering the ISFET using HP technology.

A piezoelectric ink-jet head is used for another type of ink-jet printing and consists of a small reservoir with an inlet port and a nozzle at the other end. One wall of the reservoir consists of a thin diaphragm with an attached piezoelectric crystal. When voltage is applied to the crystal, it contracts laterally, thus deflecting the diaphragm and ejecting a small drop of fluid from the nozzle. The reservoir then refills via capillary action through the inlet. One, and only one, drop is ejected for each voltage pulse applied to the crystal, thus allowing complete control over when a drop is ejected. Such devices are inexpensive and can deliver drops with volumes of tens of picoliters at rates of thousands of drops per second. In conjunction with a computer-controlled x-y stepping stage to position the array with respect to the ink-jet nozzles, it is possible to deliver different reagents to different spots on the array. Arrays of 150,000 spots can be addressed in less than one minute, with each spot receiving one drop of reagent. As pointed out above, thermal ink jets have a higher orifice density than piezoelectric printing. For more details on both types of ink-jet printing, visit http://www.hp.com/oeminkjet/tij/about.htm.

Since a computer controls the pattern of reagents as an array is being made with ink-jetting, it is as easy to make 10 arrays with different sequences as it is to make 10 identical arrays. This flexibility is perhaps the main advantage of the ink-jet approach. Achieving high density with the ink-jet approach requires one more trick. Two drops of liquid applied too closely together on

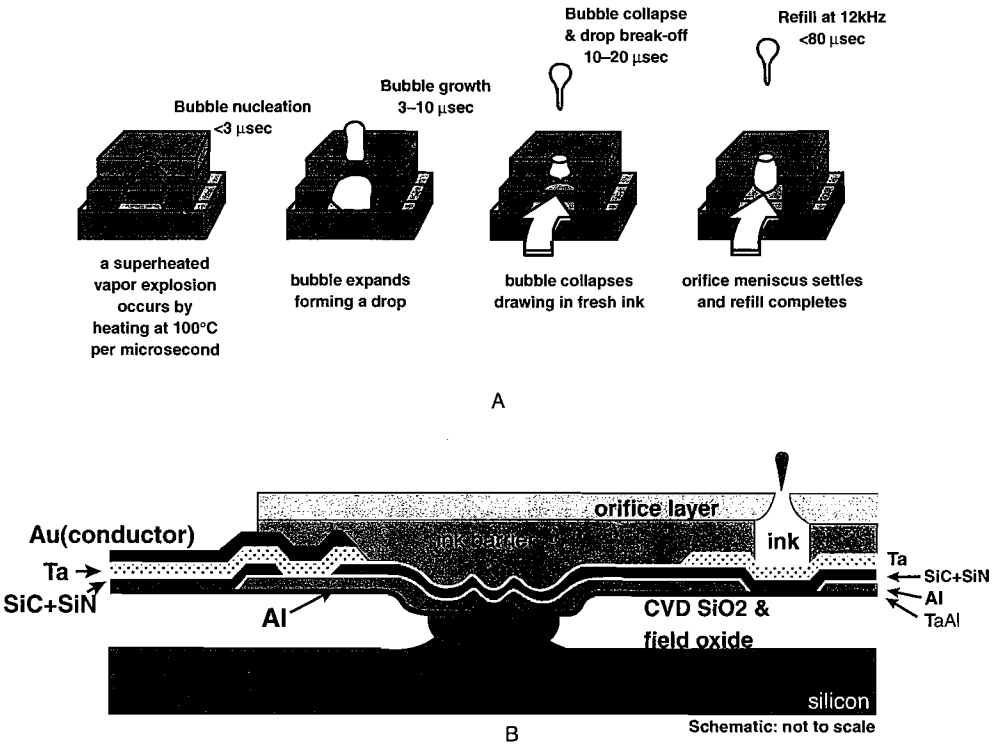

Figure 3.36 HP's Thermal Inkjet (TIJ) technology. (A) Bubble formation, expansion, collapse and refill. (B) Integrated power electronics and orifice addressing.

a surface will tend to spread into each other and mix. For 40 pL drops, the minimal center-to-center spacing is about 600 μm. This limits the array density achievable with the ink-jet method. One way around this is to engineer patterns in the surface chemistry of the array to produce spots of a relatively hydrophilic character surrounded by hydrophobic barriers. At the small length scales involved (approximately 100 μm), surface tension is the dominant force on a drop of liquid, and a hydrophobic surface will effectively prevent a drop from spreading out beyond the confines of the hydrophilic surface. There are several ways to engineer such a surface. Modern techniques use fluorinated alkyl silanes that covalently couple to glass and present an extremely hydrophobic surface. They can be patterned by masking the areas to remain hydrophilic, derivatizing the exposed surface with the appropriate silane and then removing the mask by dissolving it with various organic solvents. The mask itself can be formed by a photolithographic process wherein the array is covered with a thin, uniform layer of photoresist, which is then exposed to light through a photographic negative to define the array (see also Chapter 1). The photoresist is developed, leaving behind a pattern of protective photoresist to act as a mask. Alternatively, a "Whitesides" rubber stamp can be used to apply either the protective mask or the hydrophobic silane itself (see Chapter 1). Any of these methods will easily produce 100-μm dia. hydrophilic wells separated by 40-μm hydrophobic barriers, or 5000 array sites per cm^2. Ink-jet technology has been used to prepare microarrays of single cDNA at a density of 10,000 spots/cm^2.

On a somewhat larger scale, epoxy delivery systems used in the IC industry similarly deliver drops serially on specific spots on a substrate. A typical commercial drop-dispensing system (e.g., the Ivek Digispense 2000) delivers 0.20 to 0.50 μl in a drop and has a cycle time per dispense of 1 s. A vision system verifies substrate position and accurate dispense location to within ±25 μm of a specified location.

Ink-jetting, like silk-screening, promises to become more and more important in BIOMEMS. Earlier in this Chapter, we mentioned the current trend of using silk-screening for disposable chemical and biological sensors (see also Example 3.3). Although some inks suitable for depositing metal and dielectric films on plastics are now available, the inks for most chemical and biological organic membranes still need further research before becoming commercially available. Important additional driving forces for developing new inks for silk-screening and for ink-jetting will come from the emergence of the organic light emitting diodes (OLEDs), OLED displays and polymer transistors, and from the push toward electronic paper. In Figure 3.37 some typical thin film organic devices are shown. Using thin sheets of plastic—similar to overhead transparencies—as the base, one can print the multiple layers of OLEDs or transistors with silk-screening one layer at a time. The squeegee pushes a liquid plastic mixture over a stainless steel mesh and, after the solvent evaporates, a new plastic feature remains. So far, the smallest critical dimension achieved by Bell Labs' scientists for a printed plastic transistor is 75 μm, compared to 0.18 μm in the fastest silicon transistors (http://www.spectrum.ieee.org/publicfeature/aug00/orgs.html).

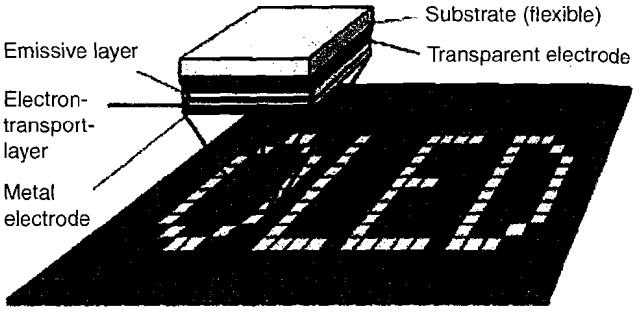

- Self-emissive
- Use of flexible substrates
- Wide viewing angle
- Ultrathin
- Low weight
- Low voltage
- High brightness
- Video speed
- Low cost manufacturing

A

B

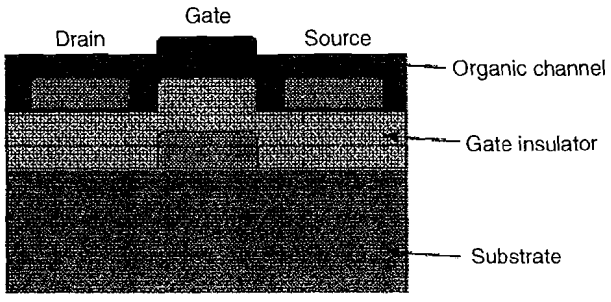

C

Figure 3.37 Organic light emitting diode (OLED). (A) In a typical organic light-emitting device, luminescent molecular excited states are generated in the electron transport and luminescent layer near its contact region with the hole transport layer. (B) OLED display; an organic passive-matrix display on a substrate of polyethylene terephthalate, a lightweight plastic, will bend around a diameter of less than a centimeter. The 1.8 mm thick, 5 by 10 cm monochrome display consists of 128 by 64 pixels, each measuring 400 by 500 μm, and is being operated at conventional video brightness of 100 cd/m^2. It was fabricated by Universal Display Corp., Ewing, N.J., with a moisture barrier built into the plastic that prevents degradation of the pixels (http://www.universaldisplay.com/). (C) Organic thin-film transistors (OTFTs) are constructed of an organic or inorganic gate insulator and an organic semiconducting channel linking the source and drain. (This figure also appears in the color plate section following page 394.)

With electronic paper, the ink is a liquid that can be printed onto nearly any surface. Within the liquid are suspended tiny microcapsules, each containing white particles and a blue dye. In an electric field, the white particles move to one end of the microcapsule and make the surface of the electronic paper appear white at that spot (Inset 3.18). An opposite electric field pulls the particles to the other end of the microcapsules, where they are obscured by the dye, making the surface appear dark at that spot. To form an electronic display, the ink is printed onto a sheet of plastic film that is laminated to a layer of circuitry. The circuitry forms a pattern of pixels that is controlled by a standard display driver (for details, log onto http://www.eink.com/technology/index.htm and http://www.edtn.com/story/tech/OEG20001130S001).

The ink-jet printing discussed above is essentially 2D, an interesting new direction is the concept of 3D printing. Stratasys uses a patented technology called *fused deposition modeling (FDM)* to build physical models by depositing semi-liquid acrylonitrile-butadiene-styrene (ABS) material in ultra-thin layers, one on top of the other (http:// www.stratasys.com/selectapart.html.) ABS offers very high strength, stiffness, and durability. It's the preferred material for making fully functional prototypes. The Stratasys 3D printer extrudes out a bead of material like a computer-controlled glue gun that leaves a three-dimensional trail.[91] As in stereolithography (also microphotoforming, see Chapter 1), one may go from computer model to manufactured product without requiring special operator training or setup.

Mechanical Microspotting

Mechanically microspotting, as developed by Shalon and Brown (Stanford University), is different from ink-jet printing. In this approach, a prepared DNA sample (e.g. cDNA or a PCR product, see Chapter 7) is loaded into a spotting pin by capillary action, and a small volume is transferred to a solid surface by physical contact between the pin and the solid substrate. After a first spotting cycle, the pin is washed and a second sample is loaded and deposited to an adjacent address. Robotic control systems and multiplexed print heads allow automated microarray fabrication. This highly flexible mechanical drop delivery technique takes a small amount of liquid from a 96 (or 384) well plate and places a tiny drop (1 nL) onto a microscope slide. Since the machine is fully automated, it requires little extra work to make additional slides. One can typically make 120 slides at a time. The microspotted microarrays currently manufactured contain as much as 10,000 groups of cDNA in an area of 3.6 cm^2. In Figure 3.38, we compare three arraying methods: lithography, microspotting, and ink-jetting. One disadvantage of microspotting and ink-jetting as compared with VLSIPS is that each sample must be synthesized, purified, and stored prior to microarray fabrication.

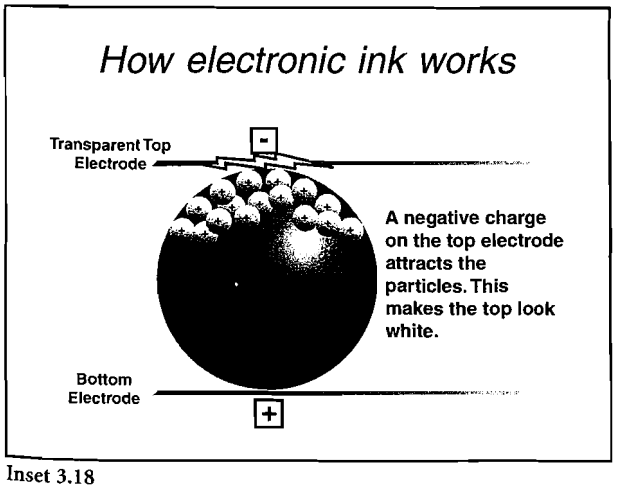

Inset 3.18

Some good websites for further information on arraying technology are Stanford University's *Brown's Lab Guide to Microarraying* at http://cmgm.stanford.edu/pbrown/mguide/ and BASF's Leming Shi's http://www.gene-chips.com/.

Micro-Contact Printing

Micro- or nano-contact printing with a PDMS stamp was reviewed in detail in Chapter 1. In this approach, a silicon master is created using high-resolution lithography. An elastomeric stamp is subsequently formed by curing an elastomeric prepolymer on this master. The resulting stamp can be inked, for example, with thiols that can be subsequently transferred to a solid support forming highly localized structured monolayers. The technique has been used, for example, to build an antibody grating on a silicon wafer by inking the rubber stamp with an antibody solution.[92] The antibody grating alone produces insignificant diffraction but, upon immunocapture of cells, the optical phase change produces diffraction. This is an alternative method to make an immunograting to the one described in Example 1.1.

Conductive Polymer Patterning

Polymers that can be electropolymerized may also be deposited and patterned by first patterning a thin-film metal electrode in a desired pattern on the substrate. In the late 1980s, this author patterned conductive polymers such as polypyrrole and polyaniline with lithography techniques. In one example, arrays of conductive polymer posts were formed on a conductive substrate. Increased materials transport to individual conductive polymer posts as compared to a uniform film of the same polymer led to higher electrochemical reversibility, which might find applications in faster polymer battery electrodes, electrochromic devices, enzyme-based biosensors, and microelectronic or molecular electronic devices. Figure 3.39 depicts the procedure for fabricating three-dimensional arrays of electronically conductive polymers as well as an SEM micrograph of the resulting patterned conductive polymer posts.[93,94]

Table 3.11 summarizes some of membrane deposition and patterning techniques.[68] At first glance, photolithography seems very promising. However, the chemistry is complex, and few results have been obtained to date, the most important exceptions being the i-STAT blood electrolyte and blood gas sensors (http://www.i-stat.com/) and the Affymax DNA arrays (http://www.affymetrix.com/). More array developers today are opting for microspotting, ink-jet printing and screen-printing as the safest and least expensive approaches.

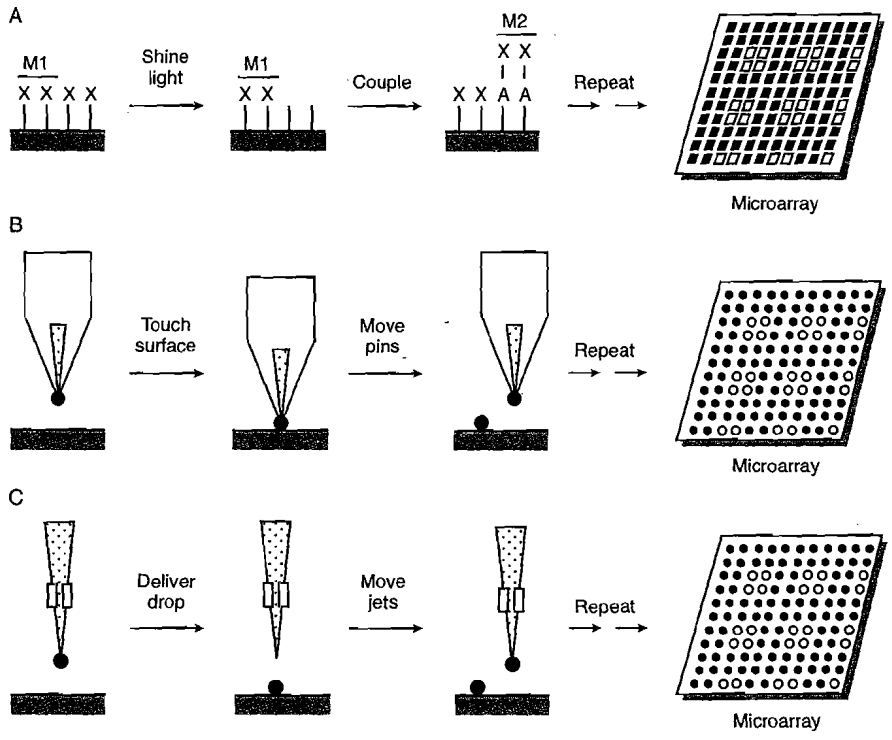

Figure 3.38 The three main arraying methods (A) lithography, (B) microspotting and (C) ink-jetting.

TABLE 3.11 Deposition and Patterning Techniques for Planar Chemical Membranes

	Typical use	Thickness range (μm)	Cost	Uniformity	Reproducibility	Patterning
Dip coating	Wire ISEs	0.1 to 50	Low	Poor	Poor	No
Casting	Planar ISEs	0.1 to >100	Low	Moderate	Moderate	No
Photolithography	Planar sensors (PVA, PHEMA)	1 to 10	Moderate	Good	Good	Yes
Lift-off	Immunosensors	0.1 to 3	Moderate	Moderate	Good	Yes
Plasma etching	PVC, Teflon®	1 to 10	High	Good	Good	Yes
Ink-jet printing	Universal	1 to 5	Moderate	Poor	Moderate	Yes
Screen-printing	Universal	5 to 50	Low	Moderate	Moderate	Yes

Source: M. Lambrechts and W. Sansen, *Biosensors: Microelectrochemical Devices*, The Institute of Physics Publishing, Philadelphia, 1992.[68] Reprinted with permission.

Thin vs. Thick Film Deposition

A comparison of thin film vs. thick film deposition is presented in Table 3.12. Resolution and minimum feature size for thin films are obviously superior. Also, the porosity, roughness, and purity of deposited metals are less reproducible with thick films. Finally, the geometric accuracy is poorer with thick films. On the other hand, the thick film method displays versatility, which is often key in chemical sensor manufacture. Silk-screening forms an excellent alternative when size does not matter but cost in relatively small production volumes does. For biomedical applications, the size limitations, clear from Table 3.12, make thick film sensors more appropriate for *in vitro* applications. For *in vivo* sensors, where size is more crucial, IC-based technologies might be more appropriate.

Thin film technology does not necessarily involve IC integration of the electronic functions. Table 3.13 provides a comparison of the economic and technical aspects in implementing thin-film technology, IC fabrication, thick film, and classic construction for sensors.[68] It should be mentioned that the sensor fabrication cost consists of 60 to 80% of packaging, an aspect not addressed in Table 3.13. In comparison with CMOS-compatible sensors, the packaging of thick film sensors usually is more straightforward. Since packaging expenses overshadow all other costs, this is a decisive criterion. In the case of chemical sensors, where the sides of the conductive Si substrate might shunt the sensing function through contact with the electrolyte, encapsulation is especially difficult compared with the packaging of an insulating plastic or ceramic substrate (see also Chapter 8).